ISSN 2812-9474

Engineering TODAY

VOL. 5 / NO. 1 / 2026

PUBLISHED BY

The Faculty of Mechanical and Civil Engineering
in Kraljevo of the University of Kragujevac

ISSN 2812-9474

VOL. 5 / NO. 1 / 2026

ET

Engineering TODAY

PUBLISHED BY

The Faculty of Mechanical and Civil Engineering
in Kraljevo of the University of Kragujevac

Engineering TODAY

PUBLISHER

The Faculty of Mechanical and Civil Engineering in Kraljevo of the University of Kragujevac

ADDRESS

Faculty of Mechanical and Civil Engineering
Dositejeva 19, 36000 Kraljevo
Republic of Serbia

CONTACT

Tel: +381 36 383 269
+381 36 383 377
+381 36 383 378

Fax: +381 36 383 269

Email: editor@engineering-today.com

Web: www.engineering-today.com

FREQUENCY

4 issues per year

PRINTED BY

SaTCIP d.o.o., Vrnjačka Banja

CIRCULATION

50 copies/issue

INSTRUCTION FOR AUTHORS

A Engineering TODAY manuscript should by written clearly and concisely in correct English. The length of a reviewing paper is up to 12 pages. All papers are subject to a reviewing process. Final acceptance of a paper for publication in the Journal is based on the decision of the Editorial Board.

TEMPLATE FOR MANUSCRIPT

Template can be downloaded from the journal's website.

SUBMISSION OF PAPERS

All manuscripts for consideration by the Engineering TODAY should be submitted via the journal's website.

CIP - Каталогизација у публикацији
Народна библиотека Србије, Београд

621(497.11)

ENGINEERING Today / editor in chief Goran Marković. - [Štampano izd.]. - Vol. 1, no. 1 (2022)- . - Kraljevo : The Faculty of Mechanical and Civil Engineering of the University of Kragujevac, 2022- (Vrnjačka Banja : SaTCIP). - 30 cm

Tromesečno. - Je nastavak: IMK-14 = ISSN 0354-6829. -
Drugo izdanje na drugom medijumu:
Engineering Today (Kraljevo. Online) = ISSN 2812-9938
ISSN 2812-9474 = Engineering Today (Kraljevo. Štampano izd.)
COBISS.SR-ID 64530953

AIMS AND SCOPE

Engineering Today is an international peer-reviewed scientific journal that publishes original papers, both theoretical and experimental, covering the whole spectrum of engineering sciences, but focusing mostly on mechanical, electrical and civil engineering. The primary objective is to provide a high-level platform for researchers and practitioners to disseminate theoretical or engineering-oriented research output achievements within the context of engineering systems that fosters knowledge sharing in different branches of engineering discipline. Engineering Today also publishes novel theoretical methods, algorithms, simulations, experiments, and case studies as applications of state-of-the-art research in the field of engineering.

The topics of interest include, but are not limited to:

- Mechanical engineering
- Electrical/electronic engineering
- Civil engineering
- Manufacturing engineering
- Software engineering
- Thermal technique and environment protection
- Applied mathematics and physics
- Theoretical and applied mechanics
- Optimization algorithms
- Metaheuristic algorithms
- Railway engineering
- Earth-moving, construction and transportation machinery
- Automatic control and fluid technique
- Computer science
- Information systems
- Fault detection and diagnosis
- Learning systems
- Robust systems
- Neuro-fuzzy systems
- Internet of things
- Cybernetics
- System identification
- Stochastic systems
- Complex networks
- Computational complexity
- Mechatronics
- Production technologies
- Computer design and computer integrated processes design
- Design of machining processes
- Engineering management and entrepreneurship
- Mechanical construction and material technology
- Interdisciplinary applications

It provides an effective medium for researchers and a way to quickly publish high-quality original papers, so as to convey the latest important progress in their professional field to scientists in related disciplines. Engineering Today offers authors rigorous peer review, rapid publication, and maximum visibility. The journal expects to accept only the most relevant manuscripts and will provide very rapid evaluation to prevent publication delays. The Editors reserve the right to reject papers without sending them out for review.

From time to time, Engineering Today will publish review articles, short communications, discussions as well as special issues on a specific sub-field of engineering science. Authors are encouraged to contact the Editor-in-Chief if they would like to submit a review article or propose and edit a special issue of the journal.

Engineering
TODAY

VOL. 5 / NO. 1 / 2026

CONTENTS

ORIGINAL SCIENTIFIC PAPER OPEN ACCESS

Optimization of sucker rod pump performance using tubing anchors

Dino Jovanović–Sovtić*[1], Eleonora Desnica[2], Stefan Stančić[1], Ana Ponoćko[1], Aleksandar Sredojević[1], Nikola Zorić[1]

[1] Scientific and technology center NIS – Naftagas

[2] University of Novi Sad, Technical Faculty "Mihajlo Pupin", Zrenjanin, Serbia

ARTICLE INFO

* **Correspondence:** dino.jovanovic@nis.rs

DOI: https://doi.org/10.5937/engtoday2600010J

UDC: 621(497.11) **ISSN:** 2812 – 9474

Article history: Received 11 March 2026; Revised 4 May 2026; Accepted 12 May 2026

ABSTRACT

Sucker rod pumps (SRPs) remain the backbone of artificial lift, yet their efficiency is undermined by tubing displacement and irregular valve operation. Tubing anchors (TA) are designed to stabilize tubing and restore stroke fidelity, but their true impact has often been generalized rather than quantified. This study delivers a systematic evaluation of TA performance using QRod 3.0 simulations across seven plunger diameters and depths from 500 to 2000 m, supported by a full calculation table of production values (Qf) with and without anchor. The results are unambiguous: TA has no measurable effect in shallow wells with small plungers, but its influence grows steadily with depth and plunger size. In mid-range configurations, anchored systems consistently outperform non-anchored ones, while in large plungers beyond 1200 m, TA becomes critical to sustaining production. At extreme depths with very large plungers, however, both anchored and non-anchored systems collapse, exposing the physical limits of SRP technology. These findings prove that TA is not a universal solution but a targeted optimization tool. Its selective application extends the operational envelope of SRPs, improves volumetric efficiency, and delivers tangible economic gains where tubing displacement is a dominant factor. The study provides operators with quantitative evidence for decision-making, replacing assumptions with data-driven justification for TA deployment.

KEYWORDS

Artificial lift, Sucker rod pump, Tubing anchor, Volumetric efficiency, QRod simulation, Production optimization, Mechanical pumping systems.

1. INTRODUCTION

Artificial lift methods are essential when reservoir pressure declines below economic production limits. Among mechanical methods - gas lift, ESP, hydraulic pumps - sucker rod pumps dominate globally, accounting for more than 80% of installations [1]. Their simplicity and adaptability make them indispensable, but efficiency losses remain a challenge.

Elastic deformation of rods and tubing causes axial displacement, leading to irregular valve operation and reduced VE [2]. Tubing anchors are designed to fix tubing at depth, reducing displacement and stabilizing pump operation [3]. The objective of this study is to quantify the impact of TA on SRP performance, evaluating both technical benefits and economic justification.

2. SUCKER ROD PUMP SYSTEM AND LIMITATIONS

SRPs operate by transferring surface mechanical energy through rod strings to a downhole plunger [4]. During operation, forces such as buoyancy, static weight, elasticity, inertia, and friction act on the system. These stresses cause tubing elongation and contraction, known as "tubing breathing," which reduces pump fillage and efficiency [5]. Figure 1 shows the complete schematic of sucker rod pump components above and below ground, including the tubing anchor.

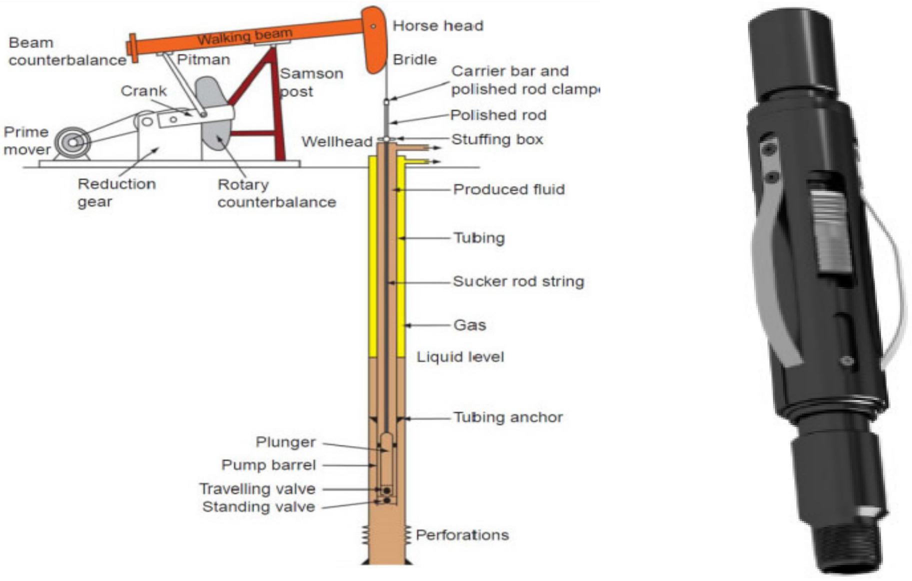

Figure 1: Schematic of sucker rod pump system and tubing anchor

Tubing anchors mitigate these effects by stabilizing tubing, improving valve timing, and ensuring faithful stroke transfer [6]. Their role becomes critical in deep wells and with larger plungers, where elastic strain and fluid column weight are significant.

3. TUBING ANCHOR

Industry literature defines TA as a device installed in the tubing string to eliminate or control axial movement caused by temperature changes, pumping cycles, and pressure fluctuations [7]. Properly designed anchors improve stability and production. Positive effects include reduced tubing displacement, improved valve operation, and higher VE [8]. However, studies warn that TA may create gas-liquid columns above the anchor, increasing pressure below and reducing pump fillage [9]. Thus, TA application must be carefully engineered for specific well conditions.

4. RESEARCH DESIGN AND METHODOLOGY

The study was based on Theoretical modeling using QRod 3.0 [10] to simulate fluid production (Qf) with and without TA across varying depths and plunger diameters. Seven plunger diameters (31.75 – 95.25 mm) were analyzed across depths from 500 to 2000 m. Constant operating parameters included stroke length, strokes per minute, tubing/casing pressures, and fluid properties. A total of 224 simulations were performed.

Table 1: Input parameters

Stroke length [mm]	1500
Strokes per minute [n/min]	5
Pump intake pressure [bar]	50
Seating depth variation [m]	500 - 2000
Tubing pressure [bar]	5
Casing pressure [bar]	5
Pump efficiency [%]	95

Volumetric efficiency was defined following Takács [11] as:

$$VE = \frac{Q_{actual}}{Q_{theoretical}} = \frac{Q_{actual}}{A_{plunger} \times S \times SPM} \quad (1)$$

Where: Q_{actual} – Daily fluid production [m^3/d], $A_{plunger}$ – Plunger area=$\pi D^2/4$ [m^2], S – Stroke lenght [m], SPM – Strokes per minute [1/m]

5. RESULTS

The following subsections detail the results for each plunger diameter. Each graph displays Q_f [m^3/day] versus seating depth, comparing performance with and without tubing anchor.

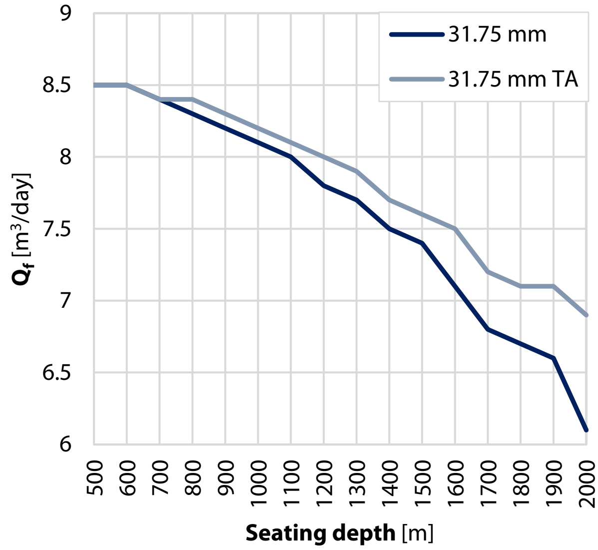

Figure 2: Production comparison with and without tubing anchor for plunger diameter 31.75 mm

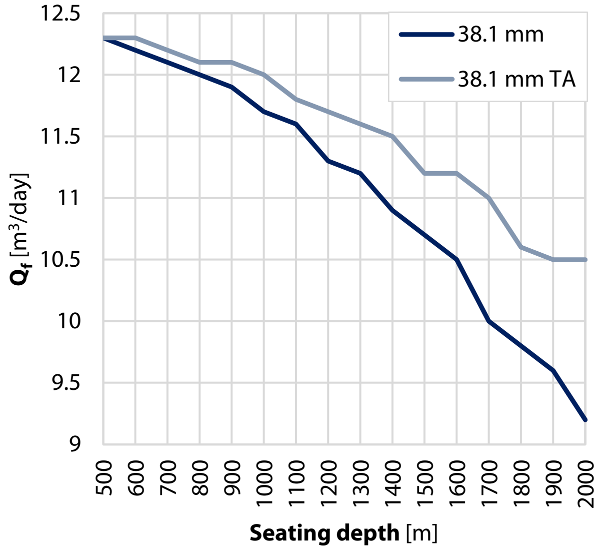

Figure 3: Production comparison with and without tubing anchor for plunger diameter 38.1 mm

At shallow depths, differences are negligible as presented in figure 2. Only beyond ~1200 m does the anchored configuration show a slight improvement, confirming that tubing displacement is not dominant for small plungers. Differences become more visible at greater depths as shown in figure 3. Anchored systems show a slower decline in production, indicating that tubing anchor begins to mitigate elastic losses in mid-range plungers.

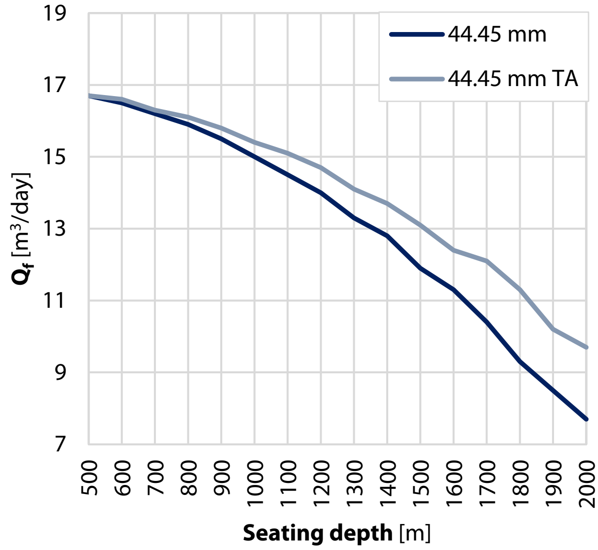

Figure 4: Production comparison with and without tubing anchor for plunger diameter 44.45 mm

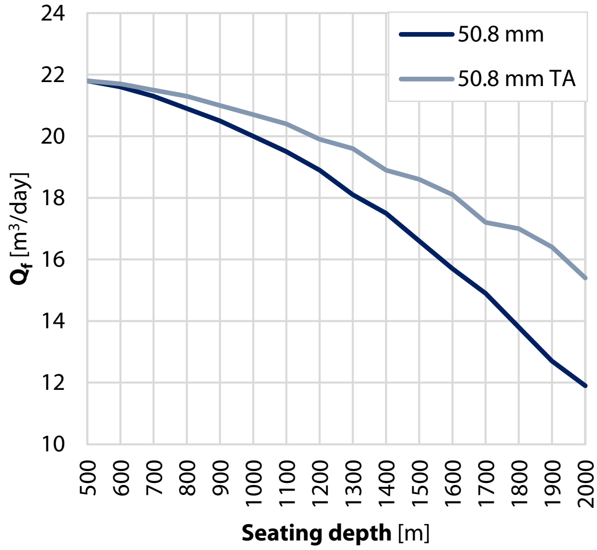

Figure 5: Production comparison with and without tubing anchor for plunger diameter 50.80 mm

Clear divergence appears at mid-depths as shown in figure 4. Anchored systems maintain higher production, demonstrating that tubing anchor stabilizes valve operation and reduces tubing elongation effects. The effect of tubing anchor intensifies with depth. Anchored systems sustain production at significantly higher levels, confirming its role in reducing tubing displacement under heavier fluid loads as shown in figure 5.

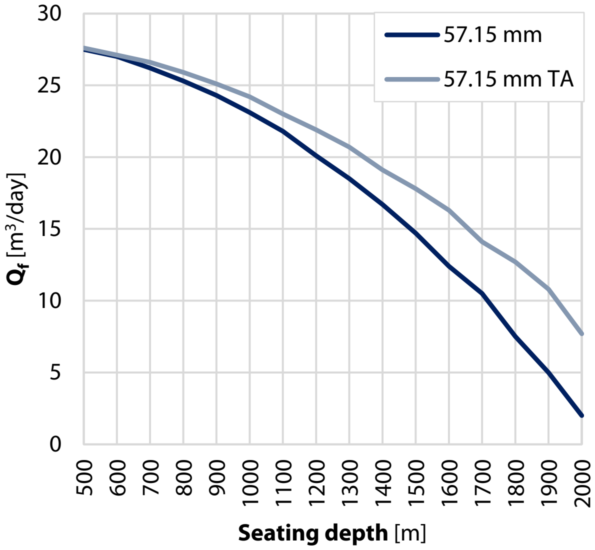

Figure 6: Production comparison with and without tubing anchor for plunger diameter 57.15 mm

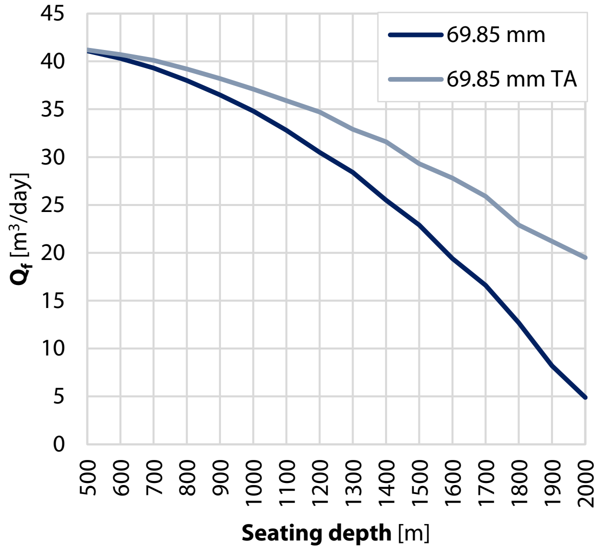

Figure 7: Production comparison with and without tubing anchor for plunger diameter 69.85 mm

Anchored systems consistently outperform non-anchored ones across all depths. As presented in figure 6, differences grow progressively larger, highlighting the anchor's contribution to preserving volumetric efficiency. Differences become dominant at depths beyond 1500 m as shown in figure 7. Anchored systems maintain production while non-anchored systems decline sharply, showing that tubing anchor is critical for large plungers in deep wells.

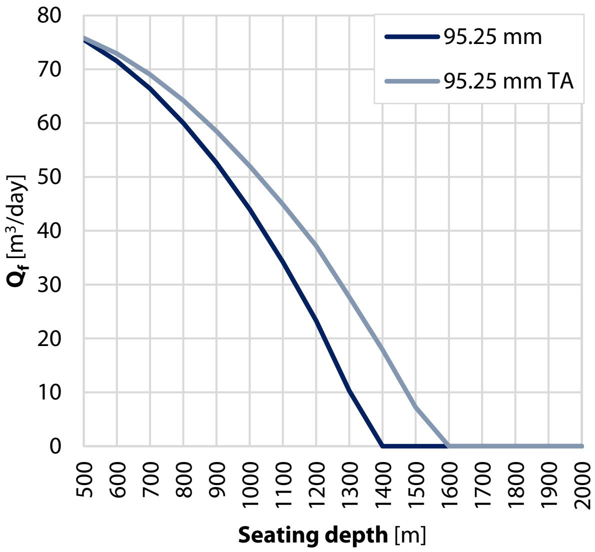

Figure 8: Production comparison with and without tubing anchor for plunger diameter 95.25 mm

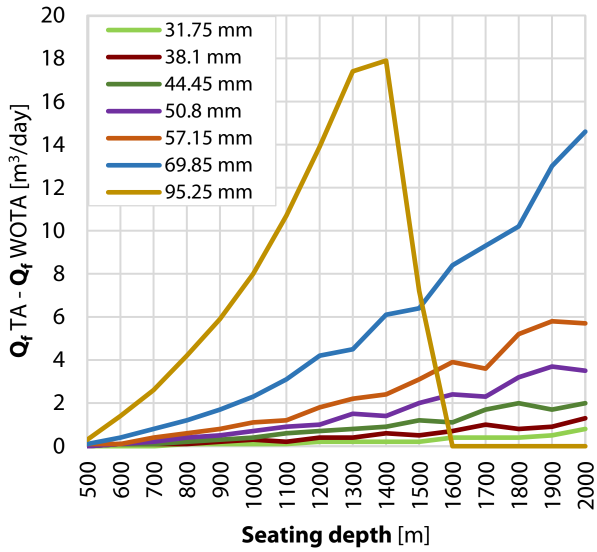

Figure 9: Production difference with/without tubing anchor for different plunger sizes at different seating depths

Anchored systems show strong benefits up to ~1600 m as presented in figure 8, but production collapses beyond this depth in both configurations. This demonstrates the physical limits of SRP systems, where tubing anchor cannot overcome extreme hydraulic constraints.

When the individual production curves for each plunger size are examined in sequence, a clear progression emerges. For the smallest plungers (31.75–38.10 mm), tubing anchor influence is minimal, with anchored and non-anchored systems producing nearly identical results across all depths. As plunger diameter increases into the mid-range (44.45–57.15 mm), the effect of tubing anchor becomes more pronounced. Anchored systems begin to show measurable improvements in production, particularly at intermediate depths, where tubing elongation and valve timing irregularities otherwise reduce efficiency.

For larger plungers (69.85 mm), the divergence between anchored and non-anchored configurations becomes substantial. At depths beyond 1200 m, anchored systems sustain production at levels significantly higher than their non-anchored counterparts, demonstrating the anchor's critical role in stabilizing tubing and preserving volumetric efficiency under heavy fluid loads. The largest plunger (95.25 mm) highlights both the benefits and the limitations of tubing anchors. Up to ~1600 m, anchored systems outperform non-anchored ones, but beyond this threshold, production collapses in both cases, revealing the physical limits of sucker rod pump systems.

Taken together, these individual graphs illustrate that the tubing anchor's impact is strongly dependent on plunger size and well depth. To better visualize the incremental benefit, the figure 9 presents the production difference (ΔQf) between anchored and non-anchored systems across all configurations. This representation isolates the anchor's contribution, highlighting the depths and plunger sizes where its application is most technically and economically justified.

6. DISCUSSION

The comprehensive set of simulations provides a clear framework for understanding how tubing anchors influence sucker rod pump performance across a wide range of operating conditions. Rather than focusing only on individual graphs, the discussion here integrates the full dataset to highlight broader technical and economic implications.

The complete calculation, shown in table 2, consolidates production values (Qf) for each plunger size at every analyzed depth, with and without tubing anchor. This dataset allows direct quantitative comparison and reveals the incremental benefit of TA in a structured way.

Table 1: Fluid production [m^3/day] calculation for different plunger sizes and different seating depths with/without use of tubing anchor

Seat. depth [m]	**31.75** Q_f	**31.75** Q_f TA	**38.1** Q_f	**38.1** Q_f TA	**44.45** Q_f	**44.45** Q_f TA	**50.8** Q_f	**50.8** Q_f TA	**57.15** Q_f	**57.15** Q_f TA	**69.85** Q_f	**69.85** Q_f TA	**95.25** Q_f	**95.25** Q_f TA
500	8.5	8.5	12.3	12.3	16.7	16.7	21.8	21.8	27.5	27.6	41.1	41.2	75.5	75.8
600	8.5	8.5	12.2	12.3	16.5	16.6	21.6	21.7	27	27.1	40.3	40.7	**71.5**	**72.9**
700	8.4	8.4	12.1	12.2	16.2	16.3	21.3	21.5	26.2	26.6	39.3	40.1	66.4	69
800	8.3	8.4	12	12.1	15.9	16.1	20.9	21.3	25.3	25.9	**38**	**39.2**	60	64.2
900	8.2	8.3	11.9	12.1	15.5	15.8	20.5	21	24.3	25.1	36.5	38.2	52.6	58.5
1000	8.1	8.2	11.7	12	15	15.4	20	20.7	**23.1**	**24.2**	34.8	37.1	44	52
1100	7.9	8.1	11.6	11.8	14.5	15.1	19.5	20.4	21.8	23	32.8	35.9	34.2	44.9
1200	7.8	8	11.3	11.7	14	14.7	**18.9**	**19.9**	20.1	21.9	30.5	34.7	23.3	37.2
1300	7.7	7.9	11.2	11.6	13.3	14.1	18.1	19.6	18.5	20.7	28.4	32.9	10.3	27.7
1400	7.5	7.7	10.9	11.5	12.8	13.7	17.5	18.9	16.7	19.1	25.5	31.6	0	17.9
1500	7.4	7.6	10.7	11.2	**11.9**	**13.1**	16.6	18.6	14.7	17.8	22.9	29.3	0	7.2
1600	7.2	7.5	10.5	11.2	11.3	12.4	15.7	18.1	12.4	16.3	19.4	27.8	0	0
1700	6.8	7.2	**10**	**11**	10.4	12.1	14.9	17.2	10.5	14.1	16.6	25.9	0	0
1800	6.6	7.1	9.8	10.6	9.3	11.3	13.8	17	7.5	12.7	12.7	22.9	0	0
1900	6.6	7.1	9.6	10.5	8.5	10.2	12.7	16.4	5	10.8	8.2	21.2	0	0
2000	**6.1**	**6.9**	9.2	10.5	7.7	9.7	11.9	15.4	2	7.7	4.9	19.5	0	0

From the table, several important patterns emerge:

- **Negligible impact in shallow wells:** For small plungers (31.75–38.10 mm), production values remain nearly identical in anchored and non-anchored configurations. This confirms that tubing displacement is not a limiting factor at shallow depths.
- **Progressive benefit in mid-range plungers:** As plunger size increases (44.45–57.15 mm), anchored systems consistently show higher Qf values, particularly at depths beyond 1000 m. This demonstrates that tubing anchor mitigates elastic losses and stabilizes valve operation.
- **Critical role in large plungers:** For 69.85 mm plungers, anchored systems maintain production at significantly higher levels, especially at depths greater than 1200 m. The table highlights that TA extends the operational envelope of SRPs, delaying efficiency collapse.
- **Limits at extreme conditions:** For the largest plunger (95.25 mm), anchored systems outperform non-anchored ones up to ~1600 m, but both configurations show sharp declines beyond this depth. The table confirms that TA cannot overcome fundamental hydraulic and mechanical constraints when system loads exceed design capacity.

By presenting the full calculation table in the Discussion, the analysis moves beyond visual trends to emphasize quantitative evidence. This approach strengthens the argument that tubing anchors are not universally required but provide substantial benefits under specific conditions.

Economically, the incremental production gains observed in the table translate into sustained fluid output, reduced downtime, and extended equipment life. Anchored systems reduce mechanical stress on rods and valves, lowering maintenance costs and improving profitability. However, the table also shows that in shallow wells or with small plungers, the anchor's contribution is negligible, meaning its installation may not be justified.

In summary, the full dataset confirms that tubing anchors are most effective in deep wells with medium to large plungers, where they stabilize system performance and preserve volumetric efficiency. Their role is limited in shallow wells and extreme depths, underscoring the need for selective application based on technical and economic evaluation.

7. CONCLUSION

This work establishes the conditions under which tubing anchors (TA) materially alter sucker rod pump (SRP) performance. By analyzing the full calculation table of production values (Qf) across seven plunger diameters and depths from 500 to 2000 m, the study demonstrates that the anchor's effect is neither uniform nor incidental, but highly dependent on system geometry and operating depth.

The data show that in shallow wells with small plungers, TA has no measurable impact: production values with and without anchor are essentially identical. In mid-range plungers, anchored systems consistently deliver higher Qf, confirming that TA mitigates elastic losses and stabilizes valve operation. For large plungers at depths beyond 1200 m, TA becomes indispensable, sustaining production levels that would otherwise decline sharply. At extreme depths with very large plungers, however, both anchored and non-anchored systems collapse, underscoring the physical limits of SRP technology.

Technically, the findings prove that TA is not a universal solution but a targeted intervention. Its selective application extends the operational envelope of SRPs, improves volumetric efficiency, and delays the onset of efficiency collapse. Economically, the incremental gains translate into sustained fluid output, reduced downtime, and extended equipment life, but only in scenarios where tubing displacement is a dominant factor.

The full calculation table provides the quantitative foundation for these conclusions, offering operators a transparent decision-making tool. Rather than relying on generalized rules of thumb, TA application can now be justified with explicit production data. Future research should validate these simulation results with long-term field measurements, investigate anchor performance under variable reservoir conditions, and integrate TA analysis into broader artificial lift selection frameworks.

REFERENCES

[1] G. Takács, Sucker-Rod Pumping Handbook: Production Engineering Fundamentals and Long-Stroke Rod Pumping, Gulf Professional Publishing, Waltham, USA, (2015).

[2] S. Fakher, A. Khlaifat, M. E. Hossain, and H. Nameer, "A comprehensive review of sucker rod pumps' components, diagnostics, mathematical models, and common failures and mitigations", Journal of Petroleum Exploration and Production Technology, Vol. 11(10), pp. 3815–3839, https://doi.org/10.1007/s13202-021-01270-7, (2021)

[3] B. Martinović, M. Bijanić, D. Danilović, A. Petrović, and B. Delibasić, "Unveiling deep learning insights: A specialized analysis of sucker rod pump dynamographs, emphasizing visualizations and human insight", Mathematics, Vol. 11(23), p. 4782, https://doi.org/10.3390/math11234782, (2023)

[4] A. Hodžić, S. Nuhanović, and D. Jovanović-Sovtić, "Improving the operation of the deep pump on piston rods by modifying the thrust valve", Journal of Faculty of mining, geology and civil engineering, Vol. 13, pp. 77-87, https://doi.org/10.51558/2303-5161.2025.13.13.77, (2025)

[5] B. Martinović, S. Stuchny, M. Repac, G. Andjusić, and N. Stevanović, "Integrated approach to optimizing wells with sucker rod pumps", PROнефть. Профессионально О Нефти, Vol. 4, pp. 64–66, https://doi.org/10.24887/2587-7399-2018-4-64- 66, (2018)

[6] M. Petrović, B. Martinović, M. Jesić, and M. Crnogorac, "Double traveling valve increases rod pump efficiency", Oil & Gas Journal, Vol. 121(12), pp. 44-49, (2023)

[7] J. Saponja, R. Hari, and F. Chaudhry, "A tubing anchor engineered to maximize production from horizontal wells", Ovintiv Technical Report, (2025)

[8] Z. Bin, G. Xianwen, and L. Xiangyu, “Complete simulation and fault diagnosis of sucker-rod pumping (includes associated comment)”, SPE Production & Operations, Vol. 36(02), pp. 277–290, https://doi.org/10.2118/204215-PA, (2021)

[9] J. N. McCoy, O. L. Rowlan, C. A. Taylor, and A. L. Podio, “Tubing anchors can reduce production rates and pump fillage”, SPE Production & Operations, Vol. 30(02), pp. 156–163, https://doi.org/10.2118/2014-1918491-PA, (2015)

[10] Weatherford International, QRod 3.0 User Manual, Houston, USA, (2015)

[11] Weatherford International, QRod 3.0 Software Documentation, Houston, USA, (2015)

ORIGINAL SCIENTIFIC PAPER OPEN ACCESS

Review on application of BIPV technology into the modern buildings

Minja Velemir Radović[1], Danijela Nikolić[1*]

[1] University of Kragujevac, Faculty of Engineering, Kragujevac, Serbia

ARTICLE INFO

[*] **Correspondence:** danijela1.nikolic@gmail.com

DOI: https://doi.org/10.5937/engtoday2600011V

UDC: 621(497.11) **ISSN:** 2812 – 9474

Article history: Received 3 April 2026; Revised 8 May 2026; Accepted 12 May 2026

ABSTRACT

Over the past few decades, there has been a noticeable increase in global energy consumption, which represents a significant problem caused by unsustainable and harmful methods of energy production. This issue leads to an emission of harmful greenhouse gases and environmental pollution on a global scale. By considering the reasons that lead to the mentioned problems, emphasis has been placed on the technologies of the renewable energy sources, as a key solution for reducing harmful environmental consequences. As a contribution to the transition to a more sustainable energy system, solar photovoltaic technology is of great importance. In addition, special attention is paid to the integration of solar photovoltaic systems into building structures (building integrated photovoltaics - BIPV). The advantage of this technology is in the balance of efficient energy saving and generation, with aesthetic and visual comfort. By analyzing the implementation of BIPV, the study provides an insight into the potential of this technology, its contribution to the global energy sustainability, as well as the results achieved through the implementation of various solutions.

KEYWORDS

Building integrated photovoltaics, Building, Application.

1. INTRODUCTION

Solar energy is the most abundant renewable energy source, available in both direct and indirect forms. Solar energy utilization can be categorized into two primary areas: solar thermal and photovoltaic systems. Solar thermal applications focus on harnessing solar radiation to produce useful heat. In contrast, photovoltaic (PV) technology is designed to convert solar energy directly into electricity, using PV cells, with conversion efficiencies ranging from 7% to 40% [1].

Photovoltaic modules are building-integrated when designed to meet essential construction requirements and replace conventional building materials. Figure 1 provides an initial overview of BIPV systems through examples. Key considerations include the type of structural integration of the modules, the flexibility in adjusting module size, and how aesthetic features can be achieved using colors, surface textures, or partially transparent designs. If the integrated PV module is removed, it will be substituted with a suitable conventional building material [2, 3].

Reducing carbon dioxide (CO2) emissions from the building sector is an urgent priority. One strategy to address this challenge is by harnessing on-site solar energy. In 2021, the growth in renewable energy generation reached its highest level in recent years, with solar PV modules contributing over 60% of this increase. More than 60% of the growth in PV usage came from utility-scale installations, while the rest was attributed to smaller systems such as commercial and residential PV modules. However, to meet global energy goals, the annual solar PV power generation will need to double over the next five years. In this context, the application of building-integrated photovoltaic (BIPV) modules into the building envelope has garnered significant research interest in enhancing building energy efficiency [4-6].

module geometry	standard size	custom size	standard width, adaptable length	custom size
appearance	close to conventional appearance, frameless modules, mounted with clamps	partially transparent, close to conventional appearance	surface texture, uniform color	sophisticated artistic design
constructional integration	additional ventilated layer	glazing-integrated	module-integrated backrail system for ventilated facades	glazing-integrated

Figure 1: Overview of BIPV systems through examples [2]

Urban morphology significantly affects the PV potential as it dictates the amount of solar radiation that can reach various parts of a building's surface. Li et al. [7] performed an analysis using a model comprising nine rectangular solids and demonstrated that buildings with higher aspect ratios and greater site coverage exhibited increased PV potential. They also found that by selecting the appropriate urban form, it is possible to achieve the annual electricity demand of a residential building. The photovoltaic (PV) potential of building facades with installed BIPV modules is significantly influenced by the pursuit of economic efficiency. Fath et al. [8] conducted an urban-scale study revealing that building façades contributed to 13% of the PV capacity necessary for achieving profitability in PV installations. In a study, Brito et al. [9] found that the PV potential of facades represented approximately 50% of the total potential when economic efficiency was not considered. However, this potential can be reduced to around 5%, 15%, and 30% if the payback period for the facade system investment is less than 17.9, 23.0, and 32.2 years, respectively.

2. CHARACTERISTICS OF BIPV

In BIPV systems, photovoltaic panels are embedded within building elements like walls or roofs. To mitigate heat buildup on the PV panels, BIPV approach involves ventilating the wall [10]. This method allows air to flow between the PV panel and the building wall, driven either by natural ventilation or forced convection, and then be expelled into the surrounding environment, as illustrated in Figure 2. Before designing a BIPV system, a thorough investigation into the different types of solar modules and the materials used in PV cells is essential to determine which module offers the best suitability, reliability, and benefits based on design, cost, and environmental factors. Additionally, an analysis of solar radiation and climatic conditions is necessary for effective integration [11-13].

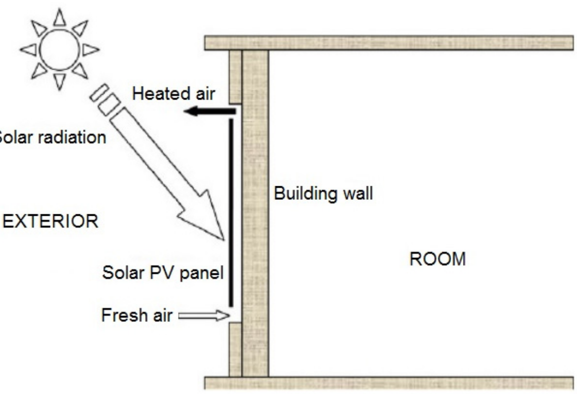

Figure 2: Schematic diagram of BIPV

The concept of BIPV has been developing over several decades. Various research groups and companies worldwide have contributed to the development of these technologies. Today, there are numerous companies and research institutions dedicated to innovating in the field of BIPV, providing new design and technological approaches to improve the efficiency and integration of solar systems into building structures.

In the early 1970s, the first initiatives and experiments related to the integration of solar systems into building structures began. The Wohnanlage Richter residential complex in Munich, Germany, designed in 1982 and featuring polycrystalline cells on its curtain walls, is recognized as one of the earliest examples of photovoltaic systems integrated into building design [14-16]. The initial attempts involved solar equipment that was added onto or installed onto existing structures. However, the real development of the BIPV concept began with the advancement of thin-film and flexible photovoltaic technologies, enabling greater adaptability and integration into various building materials. In Figure 3, a continuum of solar system designs for residential buildings is depicted, showing increasing integration (from left to right) with the architecture and materials of the building.

Figure 3: Examples of increasing integration of PV Panels [14]

BIPV systems offer exceptional long-term reliability, with typical warranties ranging from 20 to 25 years [17]. There are many advantages associated with BIPV solutions:

- innovative design,
- sun protection and electricity generation,
- minimize the building's carbon footprint,
- thermal insulation properties,
- soundproofing and enhanced comfort,
- enhance the building's value,
- eco-friendly,
- sustainability.

When considering the advantages of BIPV compared to other materials, the aesthetic appearance of these panels can be seen as both an advantage and a disadvantage. In many cases, aesthetics are crucial and significant for the adoption of BIPV in the market. Research has shown that BIPV offers improved aesthetics compared to traditional solar panels. With various BIPV technologies available, such as solar tiles, facades, glass, and solar fabrics, which are more visually appealing to architects, builders, as well as homeowners and building owners, due to their adaptability to the roofs of houses and buildings they are installed on. Aesthetic appearance is not the only important factor; it's also essential for the panels to be functional.

Although the advantages of BIPV are evident, sometimes it can be challenging to identify all the obstacles and barriers to adopting these technologies. One of the main disadvantages, according to research, is the cost. Solar tiles are more expensive than solar panels, making panels a more affordable solution for building construction. Especially when considering that the cost depends on the pitch and size of the roof on which they are installed. Another disadvantage of solar tiles relates to energy efficiency. Solar tiles sometimes have lower energy efficiency than regular solar panels, and buildings require a certain roof pitch with high sun exposure [18-19].

BIPV installations require a significant initial investment, although ongoing maintenance costs are very low. Each installation must be assessed in its unique context, especially considering the generated electrical energy, installation duration, alternative costs, etc. The cost of a BIPV installation depends on factors such as roof pitch, size, modules, design, etc. For a standard-sized single-story house, the installation cost averages around $25 per square foot. The total installation costs for solar tiles are approximately three times higher than those for solar panels, including roof reconstruction.

Many BIPV manufacturers produce custom modules manually with limited automation, leading to higher costs for solar building envelope components compared to non-solarized alternatives. This is reflected in the investment costs associated with 'handcrafted BIPV modules,' as shown in Figure 4. Currently, only a few manufacturers offer standardized BIPV products with fixed dimensions. The green dotted line at €131/m^2 represents the maximum additional cost at which solar building products remain cost-effective. If BIPV system prices fall below this line, the solar building envelope proves to be more economical over its lifespan compared to conventional options. A highly automated, flexible production process capable of producing approximately 55 MW annually, would enable pricing below €131/m^2 (including components like cabling, inverters, brackets, mounting systems, grid connections, meters, and installation). Such advancements in BIPV facade production could provide attractive profits for end users, manufacturers, and investors, and offer significant opportunities for smaller local production facilities in Europe due to the benefits of proximity and coordination with end customers [2].

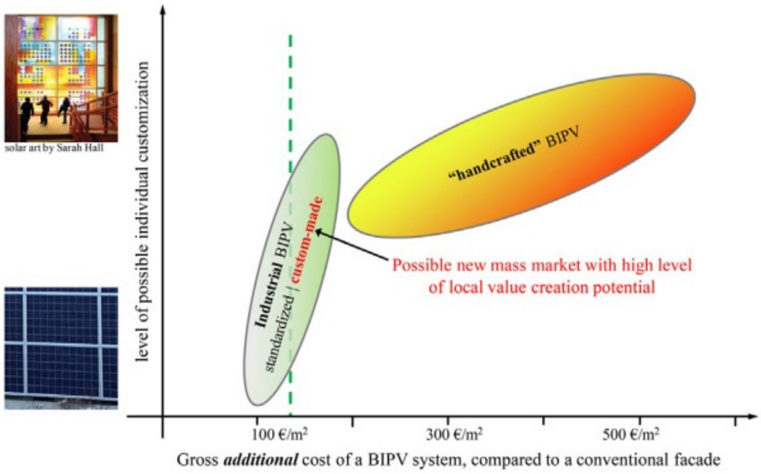

Figure 4: Additional price for a BIPV installation versus a conventional facade, depending on the degree of customization [2]

3. MAIN CATEGORIES OF BIPV

Different classifications of BIPV can be found in literature, depending on their purpose and criteria. One of the main divisions is based on the location of the installation on the building itself, so these systems can be on the roof, in the facade, or on external integrated devices. Each of these groups corresponds to application categories according to the EN 50583 standard. Roof installations correspond to categories A and B, facade installations to categories C and D, and external integrated devices to category E. Examples of BIPV systems in the building applications are shown in Figure 5.

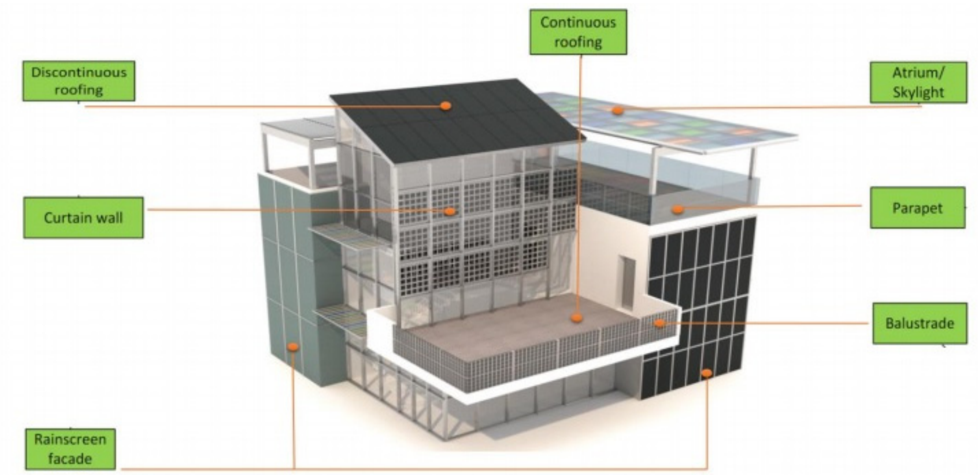

Figure 5: Examples of BIPV systems in actual building applications [20]

3.1. BIPV roof installation

Roofs unequivocally have the greatest potential for collecting solar energy, thus making them ideal for the implementation of BIPV technology. Sloped roofs, for instance around 30˚, offer the best energy collection, although flat roofs, also known as continuous roofs, can be well utilized too. One of the challenges in optimizing energy collection through solar panels is the suboptimal angle of inclination, which reduces energy production. This issue affects both types of roofs but is particularly significant for flat roofs where the inclination is inflexible or limited. Examples of BIPV installation on roofs are shown in Figure 6.

As mentioned earlier, solar roof tiles represent one of the most common ways of integrating BIPV technology. They are synonymous with traditional roof tiles. Each solar tile covers an area larger than 0.5 m^2 and can be made of foil or glaze. The resemblance of solar tiles to traditional tiles negates aesthetic challenges, seamlessly blending in with conventional flat roofs. Unlike large solar tiles, smaller ones have modules smaller than 0.5 m^2 with a configuration that does not affect their application. Roofs equipped with BIPV technology can also be (partially) transparent. These elements can cover the roof entirely or partially. Their purpose is to provide illumination to the space, along with additional thermal, sound, and water-resistant functions [20 - 23].

Figure 6: Examples of BIPV installation on roofs [24]

3.2. Façade installation of BIPV

The second significant application area of BIPV is the facade, where solar panels of all technologies can be integrated as conventional wall cladding with multiple layers and single-layer facades. Integration of solar modules into building facades can preserve the original function, security, aesthetic requirements, and facilitate electricity production throughout the year. Additionally, such a facade can reduce thermal losses from the interior of the building .

The first method of installing BIPV on the facade of a building is as a wall curtain. It involves a continuous and external system of facade openings, which can be fully or partially glazed. The term "wall curtain" refers to its construction, as the facade is suspended like a curtain from the upper edge of the building and attached at various points to prevent water and air infiltration. The construction itself is made of aluminum frames filled with glass panels. This meets various requirements such as structural support, acoustic properties, thermal insulation, water resistance, etc. This method of integrating BIPV is most common in commercial buildings. In Figure 7, an example of a commercial building with such a system installed is shown.

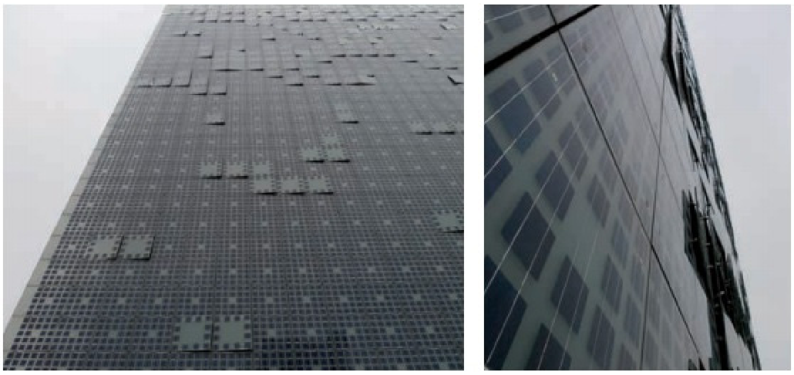

Figure 7: Curtain wall [21]

When installed as a "warm facade," this method separates the external and internal environments. It can be implemented according to various construction systems such as stick systems, unitized curtain walls, structurally glazed facades, point-fixed suspended facades. In their most basic form, these systems are windows but can also be integrated into more complex facades. Another way to install this system on the facade of a building is as a "cold" or ventilated facade. This system consists of a supporting substructure, an air gap, and cladding. It's possible to categorize them as "transparent" with openings at the top, "ventilated" with openings at the bottom and top, and "pressure-equalized" rain screen facade with barriers in the air gap. The panels are often clad in aluminum and installed a short distance from the building to allow for ventilation and drainage. The ventilation gap should be a minimum of 100mm and helps improve performance by reducing temperatures, and it can also be used as a space for cable routing. Another method is the double-skin facade, which consists of two layers, typically made of glass, with air flowing between them. The space between can range from 20mm to several meters and serves as insulation against extreme weather conditions, sound, etc. The PV is the same as in the curtain wall, but in this case, thermal insulation is not needed. One of the more intriguing methods of integrating BIPV is into the building's windows. Solar cell products designed for glazing are used for this installation method. They can come in different colors and levels of transparency, allowing for various aesthetic outcomes. The spacing between solar panels ranges from 3 to 50 mm, depending on the level of transparency and criteria for electricity production. Through this gap, daylight passes, contributing to lighting while electricity is generated. This installation method is more suitable for colder climates because in warmer regions, there might be overheating due to the greenhouse effect.

3.3. Installation of BIPV on external integrated devices

External integrated devices include building elements that come into contact only with the external environment. Therefore, BIPV can be installed on terrace railings, atriums, roller shutters, awnings, etc. Integration of PV in this manner represents one of the most effective ways to control internal daylighting and thermal conditions of the building. This reduces the penetration of solar heat into the building, leading to less need for ventilation and reducing the cooling load while providing additional electricity production. If a controllable system is installed, the louvers can track the movement of sunlight to achieve greater efficiency. Another option is to position the louvers in winter so that they collect energy during the day and close them at night to reduce heat loss [22, 23]. Examples of BIPV systems on external integrated devices are shown in Figure 8.

Figure 8: BIPV systems on external integrated devices [20]

PV panels can be integrated as multifunctional components in transparent roof structures or atriums, allowing for controlled light to enter the building's interior. As semi-transparent roof units, they provide protection from heat, sunlight, glare, and weather conditions. One integration method involves placing small PV cells on atrium glass, creating transparent gaps between them to permit controlled daylight inside. Well-designed PV-integrated atriums can also enhance the building's aesthetic from the inside. While these glazing systems are typically best suited for smaller PV installations, they can be visually appealing and offer excellent visibility. Since skylight, atrium, and greenhouse glass are often heavily tinted to reduce glare, semi-transparent PV glazing can serve as an effective alternative.

4. APPLICATION OF BIPV IN A MODERN BUILDING SECTOR

Europe used to be the largest market for PV systems worldwide, but it was recently surpassed by China. However, Europe remains the region with the highest installed PV capacity. Nevertheless, the installation rate in Europe is slowly declining while it is increasing in other leading countries worldwide. Europe continues to represent a consistent market opportunity, primarily due to the construction materials used. One of the obstacles has been the installation on historically significant buildings, concerning the color of the cells and their integration into valued facades. The problem has been solved, and on the market, cells with high integration levels and minimal visual impact are readily available. Leading the list of European countries offering the best opportunities for BIPV is Germany [25]. Projection for Europe market for the 2025th year is shown in Table 1.

Table 1: Europe market for BIPV with projection for the 2025th [25]

Application	2020	2021	2023	2025	CAGR (2020-2025)
Roofs	539.7	656.9	1,056.7	1,827.1	27.6%
Facades	321.0	366.1	516.2	780.9	19.5%
Glazing	136.3	156.1	220.6	332.2	19.5%
Shading	92.7	102.5	134.4	184.2	14.7%
TOTAL	**1,089.7**	**1,281.6**	**1,927.9**	**3,124.4**	**23.5%**

Countries in the Asia-Pacific region have recently made significant contributions to the BIPV market and have become leading markets worldwide. The reason for this is the prevalence of tiled roofs, which are common in densely populated areas of these countries, and concrete roofs, which are also very popular in this region and suitable for installing these systems. These regions host some of the leading industries for BIPV production. Looking at individual countries in this region, China stands out significantly as the largest PV consumer in recent years. Due to severe air pollution, China implemented changes to renewable energy industry laws as early as 2005. By taking such actions, the government shut down thousands of coal factories. There are also various programs for installing solar systems on a large number of government-owned houses in rural areas. Additionally, in Shanghai, every building must have a green roof, and in China, buildings must significantly reduce their energy footprint [19, 25]. Projection for Asia-Pacific region for the 2025th year is shown in Table 2.

Table 2: Asia-Pacific market for BIPV with projection for the 2025th [25]

Application	2020	2021	2023	2025	CAGR (2020-2025)
Roofs	668.6	804.3	1,264.3	2,138.7	26.2%
Facades	536.9	625.6	920.7	1,453.3	22.0%
Glazing	228.2	265.1	387.8	608.2	21.7%
Shading	87.6	97.3	129.9	184.5	16.1%
TOTAL	**1,521.3**	**1,792.3**	**2,702.7**	**4,384.7**	**23.6%**

On the American market, which includes both North and South America, roof-mounted BIPV systems have the highest usage, accounting for 80.4%, while other installation methods are represented at less than 10%. BCC Research, which analyzed the American market, highlights California, New York, New Jersey, New Mexico, Massachusetts, Pennsylvania, Maryland, Connecticut, Arizona, and Nevada as the states with the most incentives for PV systems [19, 25]. Projection for American market for the 2025th year is shown in Table 3.

Table 3: American market for BIPV with projection for the 2025th [25]

Application	2020	2021	2023	2025	CAGR (2020-2025)
Roofs	696.6	844.8	1,349.3	2,317.4	27.2%
Facades	84.3	96.0	135.3	204.3	19.4%
Glazing	27.7	30.6	39.7	53.9	14.2%
Shading	57.8	65.2	89.6	131.2	17.8%
TOTAL	**866.4**	**1,036.6**	**1,613.9**	**2,706.8**	**25.6%**

According to Aaditya et al. [26], most studies on BIPV have been conducted in controlled indoor environments or simulations, which may not accurately reflect real-world performance. The following sections explore on-site case studies of BIPV systems under actual climate conditions.

In a studies conducted by Chow et al. [27-29] in Hong Kong, a 260 m^2 BIPV wall was installed on a 30-storey subtropical hotel building, mounted on the west facade. An air gap of 250 mm was maintained between the wall and the PV panels, allowing natural ventilation through this space. Three ventilation configurations were examined: (a) PV/C, where all sides were open for ventilation; (b) PV/T, where only the top and bottom ends were open; and (c) BIPV, where PV panels were directly attached to the external wall. The PV/C configuration performed best in hotter months (April to August and October), while the PV/T configuration showed superior results during colder periods (November to February). The BIPV system excelled in September. Overall, the electrical efficiency for PV/C, PV/T, and BIPV configurations was 10.2%.

Leite, Didone and Wagner presents investigation at small section of an office building in Brazil, which was equipped with semi-transparent BIPV panels [30]. This study compared the performance of BIPV systems in Brazil with those in northern hemisphere locations. The findings revealed that the annual energy production from the semi-transparent PV system in Brazil was significantly higher than the peak energy output recorded in a German city, reaching 750.3 kWh/year, which is 39–43% greater than the highest figures reported in Germany.

Gaillard et al. [31] in France, conducted a study with three prototype building envelopes with naturally-ventilated double-skin configurations were tested on various buildings. Two of these systems were implemented on individual houses, while one was installed on an office building. The average thermal efficiency of these systems ranged from 16% during the autumn and winter months to 25% in spring and summer. For the office building façade, a temperature difference of approximately 10°C was observed, even when solar irradiation was absent.

In a study by Sadineni et al. [32] in the United States, conducted in a residential area with approximately 200 houses, the impact of photovoltaic (PV) installation orientation on peak load was investigated. The research determined that a 40° south-west orientation was the most economically favorable for consistent electricity usage and pricing. The total annual energy consumption in homes with this PV orientation was reduced by 38% compared to similarly sized homes without PV systems. Additionally, the peak energy demand for homes with PV installations decreased by 62%. In Switzerland, Jayathissa et al. [33] examined an Adaptive Solar Façade (ASF) for BIPV systems in a cold climate. The ASF significantly reduced the building's energy load, including lighting, heating, and cooling, by nearly 50% compared to a system without shading. The total energy consumption with the ASF was approximately 700 kWh.

In a study by Chatzipanagi et al. [34] in Switzerland, BIPV systems were demonstrated as both window and roof installations, with variations including systems with and without air gaps for ventilation. The study focused on how PV cell operating temperature affected performance, using models such as NOCT and Equivalent Cell Temperature (ECT). It was found that a c-Si module inclined at 30° outperformed one inclined at 90° across all seasons, primarily due to shadow effects impacting the latter. This highlights the significant role of installation angles and seasonal variations in the performance of BIPV systems.

The following examples are not necessarily the most aesthetically pleasing or functional building solutions, but they illustrate the successful application of PV systems across various geographical, cultural, and climatic contexts.

On the southern side of the Meier Hospital in Florence, a photovoltaic glass tower was constructed to maximize solar energy collection, particularly during the winter months. This project was designed by the firm CSPA Firenze, led by architect Paolo Felli. Besides considering energy and environmental aspects, attention was also given to social impact. Figure 9 depicts the glass tower.

Figure 9: PV glass tower of the Meier Hospital [21]

The aim was to create a pleasant space without additional energy usage that would be in use for various activities throughout most of the year. Integrating PV installations into the facades of the glass tower building allows for combining energy production with other functions of the building envelope. Electrical energy is generated on-site, avoiding losses in transmission and distribution and reducing capital and maintenance costs for the electricity distribution company. The PV system has a capacity of 30 kWp and is implemented with glass/glass PV modules.

The Greeting to the Sun monument is located in Zadar, next to the sea, and it was designed by Nikola Bašić. The monument has a diameter of 1102 mm and symbolizes the sun, which absorbs sunlight through solar panels during the day and then transforms that energy into visual effects during the night, as shown in Figure 10. This artistic installation contains over 300 multilayered glass plates, with a photovoltaic solar module [21].

Figure 10: Monument „Greeting to the Sun" in Zadar [21]

Below the glass, there are over a thousand lights that can illuminate with different intensities and colors. Using a computer, various messages, graffiti, words, etc., can be displayed here. In the future, it is planned that entering the circle would trigger a light reaction, which would interact further if more people are present within the circle.

The Sheikh Zayed Learning Center is located in Abu Dhabi and had to meet a series of requirements set by the urban planning council. By fulfilling all these requirements, this center became the first state building to achieve the highest possible sustainability rating. The building was designed to be energy-independent, achieved through a combination of the best available lighting and ventilation techniques. Sheikh Zayed Learning Center is shown in Figure 11.

The building is designed to facilitate airflow circulation through and around the courtyard, as well as to maximize the use of sunlight. Small windows allow for natural light while avoiding excessive solar radiation. The structure is predominantly embedded in the ground to reduce temperature differentials between the interior and exterior. BIPV collectors are installed across the entire roof surface, generating 150 kW. This way, the building produces 95 percent of its required energy [21].

Figure 11: Sheikh Zayed Learning Center in Abu Dhabi [21]

5. CONCLUSION

Excessive energy consumption represents a key challenge in sustainability and environmental protection. To combat this, measures need to be taken to increase energy efficiency, promote renewable energy sources, and reduce unnecessary energy waste. The use of solar energy, as a form of renewable energy, has proven to be particularly effective. Special emphasis has been placed on integrating BIPV into structures to achieve efficiency and aesthetic value.

BIPV technology has significant potential to transform the construction industry and contribute to the sustainability of urban development. The integration of solar panels into buildings enables the production of clean energy on-site, reduces emissions of harmful gases, and decreases dependence on traditional energy sources. Additionally, BIPV systems offer aesthetic and functional benefits, contributing to modern and innovative building design. These systems have the potential to greatly enhance building performance while also reducing harmful emissions. It is important to assess the energy loads required by type during both the design and operational phases of a building. Additionally, choosing appropriate materials and determining the optimal placement of systems within the building are crucial steps for maximizing the effectiveness of this technology.

However, despite numerous advantages, several challenges limit the wider implementation of BIPV technology, including high initial costs, lack of standardization, regulatory barriers, and insufficient awareness of potential benefits. To overcome these challenges, further research and development in the field of BIPV are necessary to enable wider implementation of these innovative systems.

ACKNOWLEDGEMENTS

This work was supported by the Ministry of Education, Science and Technological Development of the Republic of Serbia through the Agreements No. 451-03-33/2026-03/200107 and No. 451-03-34/2026-03/200107.

REFERENCES

[1] M. Debbarma, K. Sudhakar, and P. Baredar, "Comparison of BIPV and BIPVT: A review", Resource-Efficient Technologies, Vol. 3(3), pp. 263–271, https://doi.org/10.1016/j.reffit.2016.11.013, (2017)

[2] E. Kuhn, C. Erban, M. Heinrich, J. Eisenlohr, F. Ensslen, and D. H. Neuhaus, "Review of technological design options for building integrated photovoltaics (BIPV)", Energy and Buildings, Vol. 231, p. 110381, https://doi.org/10.1016/j.enbuild.2020.110381, (2021)

[3] IEC, "Photovoltaics in Buildings – Part 1: Building-Integrated Photovoltaic Modules", Committee Draft 63092-1, IEC Central Office, Switzerland, (2020)

[4] IEA, "Renewables 2021 – Analysis and Forecast to 2026", https://iea.blob.core.windows.net/assets/5ae32253-7409-4f9a-a91d-1493ffb9777a/Renewables2021-Analysisandforecastto2026.pdf, (2021)

[5] E. Saretta, P. Bonomo, and F. Frontini, "A calculation method for the BIPV potential of Swiss façades at LOD2.5 in urban areas: A case from Ticino region", Solar Energy, Vol. 195, pp. 150–165, https://doi.org/10.1016/j.solener.2019.11.062, (2020)

[6] N. Martín-Chivelet, K. Kapsis, H. R. Wilson, V. Delisle, R. Yang, L. Olivieri et al., "Building-Integrated Photovoltaic (BIPV) products and systems: A review of energy-related behavior", Energy and Buildings, Vol. 262, p. 111998, https://doi.org/10.1016/j.enbuild.2022.111998, (2022)

[7] D. Li, G. Liu, and S. Liao, "Solar potential in urban residential buildings", Solar Energy, Vol. 111, pp. 225–235, https://doi.org/10.1016/j.solener.2014.10.045, (2015)

[8] K. Fath, J. Stengel, W. Sprenger, H. R. Wilson, F. Schultmann, and T. E. Kuhn, "A method for predicting the economic potential of (building-integrated) photovoltaics in urban areas based on hourly Radiance simulations", Solar Energy, Vol. 116, pp. 357–370, https://doi.org/10.1016/j.solener.2015.03.023, (2015)

[9] M. C. Brito, S. Freitas, S. Guimaraes, C. Catita, and P. Redweik, "The importance of facades for the solar PV potential of a Mediterranean city using LiDAR data", Renewable Energy, Vol. 111, pp. 85–94, https://doi.org/10.1016/j.renene.2017.03.085, (2017)

[10] S. S. S. Baljit, H. Y. Chan, and K. Sopian, "Review of building integrated applications of photovoltaic and solar thermal systems", Journal of Cleaner Production, Vol. 137, pp. 677–689, https://doi.org/10.1016/j.jclepro.2016.07.150, (2016)

[11] J. P. Kalejs, "Silicon ribbons and foils—state of the art", Solar Energy Materials and Solar Cells, Vol. 72, pp. 139–153, https://doi.org/10.1016/s0927-0248(01)00159-3, (2002)

[12] G. N. Tiwari, R. K. Mishra, and S. C. Solanki, "Photovoltaic modules and their applications: A review on thermal modelling", Applied Energy, Vol. 88(7), pp. 2287–2304, https://doi.org/10.1016/j.apenergy.2011.01.005, (2011)

[13] T. T. Chow, "A review on photovoltaic/thermal hybrid solar technology", Applied Energy, Vol. 87(2), pp. 365–379, https://doi.org/10.1016/j.apenergy.2009.06.037, (2010)

[14] T. James, A. Goodrich, M. Woodhouse, R. Margolis, and S. Ong, "Building-Integrated Photovoltaics (BIPV) in the Residential Sector: An Analysis of Installed Rooftop System Prices", Technical Report, National Renewable Energy Laboratory, (2011)

[15] P. Corti, P. Bonomo, F. Frontini, P. Mace, and E. Bosch, "Building Integrated Photovoltaics: A Practical Handbook for Solar Buildings' Stakeholders", SUPSI – Swiss BIPV Competence Centre, (2020)

[16] T. Chen, Y. An, and C. K. Heng, "A review of building-integrated photovoltaics in Singapore: Status, barriers, and prospects", Sustainability, Vol. 14(16), p. 10160, https://doi.org/10.3390/su141610160, (2022)

[17] T. N. Anderson, M. Duke, G. L. Morrison, and J. K. Carson, "Performance of a building integrated photovoltaic/thermal (BIPVT) solar collector", Solar Energy, Vol. 83(4), pp. 445–455, https://doi.org/10.1016/j.solener.2008.08.013, (2009)

[18] W. Ahmed, J. A. Sheikh, T. Kerekes, and M. A. P. Mahmud, "Solar roof tiles: Unleashing technical advantages and contribution to sustainable society", Science of The Total Environment, Vol. 954, p. 176818, https://doi.org/10.1016/j.scitotenv.2024.176818, (2024)

[19] K. Johnson, E. Gough, and J. C. Servo, "Building Integrated Photovoltaics", New York, (2021)

[20] IEA-PVPS, "Categorization of BIPV Applications", IEA-PVPS T15-12:2021, (2021)

[21] M. Achenza and G. Desogus, "Guidelines on Building Integration of Photovoltaic in the Mediterranean Area", ENPI CBC Mediterranean Sea Basin Programme, Cagliari, (2019)

[22] P. Bonomo, A. Chatzipanagi, and F. Frontini, "Overview and analysis of current BIPV products: new criteria for supporting the technological transfer in the building sector", International Journal of Architectural Technology and Sustainability, Vol. 1, pp. 67–85, https://doi.org/10.4995/vitruvio-ijats.2015.4476, (2015)

[23] E. Rodriguez-Ubinas, E. Trepc, and N. Alhammadi, "Classification of photovoltaics in buildings (bapv and bipv): illustrated with zero-energy houses", WIT Transactions on Ecology and the Environment, Vol. 260, pp. 37–50, (2022)

[24] P. Heinstein, C. Ballif, and L. E. Perret-Aebi, "Building Integrated Photovoltaics (BIPV): Review, Potentials, Barriers and Myths", Green, Vol. 3(2), pp. 125–156, https://doi.org/10.1515/green-2013-0020, (2013)

[25] BCC Research, "Building-Integrated Photovoltaics (BIPV): Technologies and Global Markets", Report EGY072B, BCC Research, (2021)

[26] G. Aaditya, R. Pillai, and M. Mani, "An insight into real-time performance assessment of a building integrated photovoltaic (BIPV) installation in Bangalore (India)", Energy for Sustainable Development, Vol. 17, pp. 431–437, https://doi.org/10.1016/j.esd.2013.04.007, (2013)

[27] T. T. Chow, A. L. S. Chan, K. F. Fong, Z. Lin, W. He, and J. Ji, "Annual performance of building-integrated photovoltaic/water-heating system for warm climate application", Applied Energy, Vol. 86, pp. 689–696, https://doi.org/10.1016/j.apenergy.2008.09.014, (2009)

[28] T. T. Chow, J. W. Hand, and P. A. Strachan, "Building-integrated photovoltaic and thermal applications in a subtropical hotel building", Applied Thermal Engineering, Vol. 23(16), pp. 2035–2049, https://doi.org/10.1016/s1359-4311(03)00183-2, (2003)

[29] T. T. Chow, W. He, and J. Ji, "An experimental study of façade-integrated photovoltaic/water-heating system", Applied Thermal Engineering, Vol. 27, pp. 37–45, https://doi.org/10.1016/j.applthermaleng.2006.05.015, (2007)

[30] E. L. Didone and A. Wagner, "Semi-transparent PV windows: a study for office buildings in Brazil", Energy and Buildings, Vol. 67, pp. 136–142, https://doi.org/10.1016/j.enbuild.2013.08.002, (2013)

[31] L. Gaillard, S. Giroux-Julien, C. Menezo, and H. Pabiou, "Experimental evaluation of a naturally ventilated PV double-skin building envelope in real operating conditions", Solar Energy, Vol. 103, pp. 223–241, https://doi.org/10.1016/j.solener.2014.02.018, (2014)

[32] S. B. Sadineni, F. Atallah, and R. F. Boehm, "Impact of roof integrated PV orientation on the residential electricity peak demand", Applied Energy, Vol. 92, pp. 204–210, https://doi.org/10.1016/j.apenergy.2011.10.026, (2012)

[33] P. Jayathissa, M. Jansen, N. Heeren, Z. Nagy, and A. Schlueter, "Life cycle assessment of dynamic building integrated photovoltaics", Solar Energy Materials and Solar Cells, Vol. 156, pp. 75–82, https://doi.org/10.1016/j.solmat.2016.04.017, (2016)

[34] A. Chatzipanagi, F. Frontini, and A. Virtuani, "BIPV-temp: a demonstrative building integrated photovoltaic installation", Applied Energy, Vol. 173, pp. 1–12, https://doi.org/10.1016/j.apenergy.2016.03.097, (2016)

ORIGINAL SCIENTIFIC PAPER OPEN ACCESS

Wind speed modeling in wind energy based on one year of SCADA data using statistical distribution functions

Gojko Krunić[1*], Srđan Vasković[2], Srećko Krile[3]

[1] University of East Sarajevo, Faculty of Production and Management, Trebinje, Bosnia and Herzegovina

[2] University of East Sarajevo, Faculty of Mechanical Engineering, East Sarajevo, Bosnia and Herzegovina

[3] Srećko Krile, RP Global projekti d.o.o., Zagreb, Croatia

ARTICLE INFO

[*] **Correspondence:** gojko.krunic@fpm.ues.rs.ba

DOI: https://doi.org/10.5937/engtoday2600012K

UDC: 621(497.11) **ISSN:** 2812-9474

Article history: Received 1 April 2026; Revised 25 May 2026; Accepted 28 May 2026

ABSTRACT

Wind speed is one of the basic meteorological parameters in the field of wind energy, as it directly affects the efficiency and output power of wind turbines. Wind speed distribution is most often modeled using statistical functions, in particular the probability density function (PDF) and the cumulative distribution function (CDF). In this paper, a comparison of several statistical distributions (Weibull, Rayleigh, gamma, normal and beta) was performed through the analysis of the empirical distribution of wind speed recorded over a one-year period. For all distributions, the root mean square error (RMSE) and the mean absolute error (MAE) between observed and modeled values were calculated, and the smallest values of these criteria were used to identify the model that most accurately describes the actual wind behavior at the observed location. The obtained results enable a more precise assessment of the wind speed distribution and the energy potential of the location, which is of key importance for optimizing the operation of wind energy systems.

KEYWORDS

Wind speed, Statistical modeling, Probability density function, Cumulative distribution function, RMSE, MAE

1. INTRODUCTION

Winds are a significant component of the climate system and are closely intertwined with our daily lives. They vary over a wide range of spatial and temporal scales, from global to regional winds, to locally smaller turbulent eddies [1]. The energy sector is under increasing pressure to address the chal- lenges of climate change and the growing demand for energy. In this context, the transition to sustainable and environmentally friendly en- ergy sources has become essential for long-term stability and develop- ment [2]. Wind energy is one of the fastest growing renewable energy sources (RES) that have been developed as an efficient response to growth and global economic development over the decades [3]. Wind energy, a renewable energy source, is becoming increasingly popular and is among the priority investment areas for many countries [4].

Although the benefits of harnessing wind energy are obvious, implementation can be subject to a number of practical difficulties and uncertainties, one of which is the intermittent and unstable nature of wind [5]. The chaotic nature of wind speed poses modeling difficulties [6]. Wind energy availability and conversion efficiency depend on the distribution of wind speed [7]. The distribution of wind speed is of great importance in the assessment of wind resources, and not just the average wind speed. In order to adequately describe the variation of wind energy, it is necessary to fit various probability functions to field data, and therefore the distribution of wind energy is represented by standard statistical functions [8]. The global transition to sustainable energy has become imperative due to the rapid depletion of fossil fuel resources and the serious environmental consequences associated with greenhouse gas emissions [9].

Wind energy represents one of the key directions of development of renewable energy sources, aimed at reducing emissions of harmful gases and increasing energy efficiency. The efficiency of wind power plants is significantly determined by the characteristics of the wind, with wind speed representing a key parameter in assessing the energy potential of a location and selecting the optimal wind turbine. Since wind energy is proportional to the cube of wind speed, it means that even a small increase in wind speed results in a large increase in wind energy, therefore the most important factor affecting wind energy is wind speed [10]. SCADA (Supervisory Control and Data Acquisition - SCADA) is a control system architecture that uses computers, networked data transmission, and graphical user interfaces for high-level process control [11]. Wind farms are connected to a SCADA system to continuously collect wind turbine data [12].

The main factors affecting wind speed and direction are the pressure gradient force, the Coriolis force, and friction with the Earth's surface [13]. Since wind speed is a random variable that varies in time and space, its statistical modeling is of key importance for the accurate assessment of wind energy potential. For this purpose, various statistical distributions are applied, with the Weibull, Rayleigh, gamma, normal, and beta distributions being the most commonly used. Their characteristics are analyzed using the probability density function and the cumulative distribution function. To assess the quality of fitting theoretical distributions to empirical data, statistical error criteria are used, including RMSE and MAE. These indicators quantitatively measure the deviation between empirical and theoretical distribution values, with smaller RMSE and MAE values indicating a better fit of the model to the actual data. Accordingly, the distribution with the smallest values of these criteria is considered the most appropriate for describing the actual behavior of wind speed at the observed location.

The aim of this paper is to conduct a detailed comparative analysis of multiple statistical distributions based on one-year wind speed measurements, with a special emphasis on identifying the model that most accurately describes the empirical data and best approximates the actual wind speed distribution at the observed location. By comparing different theoretical distribution functions and adapting them to experimental data, a deeper understanding of wind characteristics and its variability during the year is gained. The obtained results contribute to increasing the accuracy of wind energy potential estimation, which is crucial for proper planning and dimensioning of wind energy plants. At the same time, they provide guidelines for more efficient management and optimization of wind energy systems, with the aim of achieving maximum energy efficiency and economic justification of investments. The scientific contribution of this paper is reflected in the comparative analysis of multiple statistical distributions based on real SCADA data, with the application of RMSE and MAE criteria for selecting the optimal wind speed distribution model.

2. METHODOLOGY

2.1. Location and description of the wind farm

The wind speed data used in this paper were collected at the Rudine wind farm in Croatia. The wind farm is located at Rudine, at an altitude ranging from 280 to 400m above sea level. The initial project planned the construction of 34 wind turbines, of which 12 wind turbines have been completed so far, along with the accompanying infrastructure in the form of access roads and operational plateaus. The project amendments envisage a reduction in the total number of wind turbines to 18, while at the same time reducing the area of the aforementioned infrastructure. The location of the existing and planned wind power plant "Rudine" is shown in Figure 1 [14].

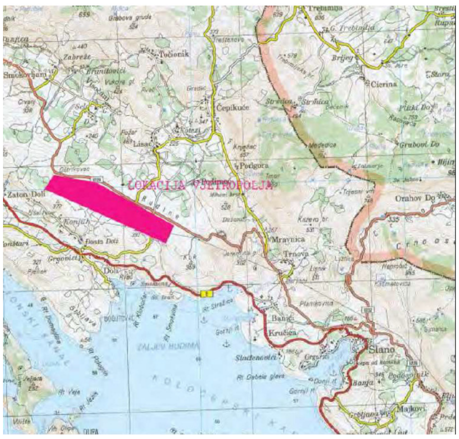

Figure 1: Location of the existing and planned wind power plant "Rudine"

The planned location of the wind turbines within the "Rudine" wind power plant is shown in Figure 2 [14].

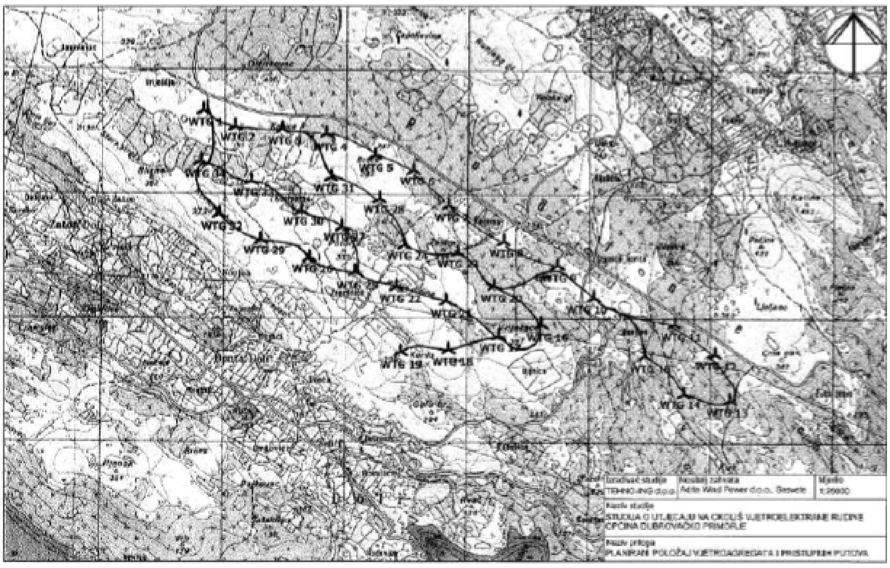

Figure 2: Planned location of wind turbines within the "Rudine" wind farm

2.2. Data collection

The wind turbines are connected to a SCADA system, which enables continuous collection of operational data. Wind speed measurements were made using an anemometer placed at a height of 85m above the ground, with a time resolution of 10 minutes. A total of 630113 measurements were collected over a one-year period. For the purposes of analysis, a representative set of 63013 records was formed using equidistant sampling, with every tenth data point selected.

The paper analyzes wind speeds collected from the WTG 27 wind turbine. Based on these data, statistical processing and modeling of the wind speed distribution was performed using several theoretical functions, including Weibull, Rayleigh, gamma, normal and beta distributions. Each distribution is defined by an appropriate set of parameters, the estimation of which allows for a precise description of the statistical characteristics of the wind speed.

2.3. Model evaluation

To assess the quality of the fit of theoretical distributions to empirical data, statistical error criteria were used, including root mean square error (RMSE) and mean absolute error (MAE), with smaller values of these criteria indicating better agreement of the model with the actual data. Analysis of probability density functions and cumulative distribution functions allows identification of the distribution that most accurately describes the empirical wind speed distribution and provides a reliable basis for assessing the wind energy potential of the observed location.

3. MATHEMATICAL FUNDAMENTALS OF DISTRIBUTION FUNCTIONS

Statistical distributions are a key tool for quantitative modeling and analysis of variable natural phenomena, with wind speed being one of the most important parameters in the field of wind energy. For each distribution, a probability density function and a cumulative distribution function can be determined.

Wind energy applications require accurate resource estimation, which can be achieved by a probability density function that describes the behavior of the wind [15]. Probability density functions (PDFs) are mathematical functions that characterize the likely behavior of a data set. This data set can correspond to the behavior of a random variable that is continuous in time. Since wind speed is a random variable, it is convenient to describe it using PDFs [16]. The probability density function *f(x)* of a continuous random variable *X* is the first derivative of the cumulative distribution function *F(x)* and is represented by the following equation [17]:

$$f(x)=\frac{d}{dx}F(x) \quad (1)$$

The cumulative distribution function for a random variable *X* is the mathematical function $F_X : R \rightarrow [0,1]$, which associates with each real number *x* the probability that the random variable *X* will take a value less than or equal to that value. The cumulative distribution function is represented by the following equation [17]:

$$F_X(x) = \Pr(X \leq x) \quad (2)$$

where:

$F_X(x)$ - cumulative distribution function of a random variable X, and Pr $(X \leq x)$ - denotes the probability that X takes on a value less than or equal to x.

The mathematical foundations of the distribution functions for Weibull, Rayleigh, gamma, normal, and beta distributions are presented below.

3.1. Weibull distribution

The most commonly used statistical approach to predict the distribution of wind speed data is the Weibull probability density function. The Weibull distribution is a distribution with greater sensitivity and greater flexibility than other distributions [18]. The two-parameter Weibull and Rayleigh distributions are widely used as statistical methods in modeling wind speed data [6]. Currently, the two- or three-parameter Weibull distribution is widely used in wind energy engineering to estimate the expected level of electricity generation [19].

The Weibull distribution is often applied in wind energy because of its ability to model different forms of wind speed distribution. The probability density function of a two-parameter Weibull distribution is represented by the following equation [20]:

$$f(x)=\frac{\beta}{\eta}\left(\frac{x}{\eta}\right)^{\beta-1} e^{-\left(\frac{x}{\eta}\right)^{\beta}}, \beta>0, \eta>0 \tag{3}$$

where:

η - scale parameter and β - shape parameter.

The cumulative function of the two-parameter Weibull distribution is represented by the following equation [21]:

$$F(t)=1-\exp\left[-\left(\frac{t}{\alpha}\right)^{\beta}\right], t\geq 0 \tag{4}$$

where:

$F(t)$ - probability that the random variable T (wind speed) takes on a value less than or equal to t, $t \geq 0$ - values for which the function is defined, α - scale parameter and β - shape parameter.

The scale parameter determines the horizontal stretching of the distribution, with a larger value of the scale parameter resulting in a wider range of values. The shape parameter determines the shape of the distribution.

3.2. Rayleigh distribution

The probability density function of the Rayleigh distribution is represented by the following equation [22]:

$$f(x;a)=\frac{x}{\alpha^2} e^{-\frac{x^2}{2\alpha^2}} \tag{5}$$

The cumulative Rayleigh distribution function is represented by the following equation [22]:

$$F(x)=\int_0^x f(y)dy=\frac{1}{\alpha^2}\int_0^x ye^{-\frac{y^2}{2\alpha^2}}dy=\int_0^{\frac{x^2}{2\alpha^2}} e^{-z}dz=1-e^{-\frac{x^2}{2\alpha^2}} \tag{6}$$

where:

x - variable from the set of real positive numbers and a - scale parameter.

3.3. Gamma distribution

The probability density function of the gamma distribution is represented by the following equation [23]:

$$f(x_i)=\frac{1}{scale^{shape}\Gamma(shape)}x_i^{(shape-1)}e^{-\left(\frac{x_i}{scale}\right)} \tag{7}$$

where:

x_i - random variable, *shape* - gamma distribution shape parameter ($k > 0$), *scale* - gamma distribution scale parameter ($\Theta > 0$) and G(*shape*) - gamma function.

The cumulative gamma distribution function is represented by the following equation [22]:

$$F(x)=\int_0^x f(x)dx=\frac{a^b}{\Gamma(b)}\int_0^x u^{b-1}e^{-au}du=\frac{a^b}{\Gamma(b)}\int_0^{ax}\left(\frac{v}{a}\right)^{b-1}e^{-v}\frac{dv}{a}=\frac{1}{\Gamma(b)}\int_0^{ax}v^{b-1}e^{-v}dv=\frac{\gamma(b,ax)}{\Gamma(b)} \quad (8)$$

where:

x - random variable, *f*(*u*) - probability density function of gamma distribution, *a* - rate parameter, *b* - shape parameter, *Γ*(*b*) - gamma function and *γ* (*b, ax*) - incomplete gamma function.

3.4. Normal distribution

The probability density function of a normal distribution is represented by the following equation [22]:

$$f\left(x;\mu,\sigma^2\right)=\frac{1}{\sigma\sqrt{2\pi}}e^{-\frac{1}{2}\left(\frac{x-\mu}{\sigma}\right)^2} \quad (9)$$

where:

x - random variable, *μ* - location parameter and *σ* - standard deviation.

A normal distribution with a location parameter equal to zero and a standard deviation *σ* = 1 is called a standard normal distribution. The cumulative function of the standard normal distribution is represented by the following equation [22]:

$$F(z)=\begin{cases}\frac{1}{2}+\frac{1}{2}P\left(\frac{1}{2},\frac{z^2}{2}\right) & \text{if } z\geq 0\\ \frac{1}{2}-\frac{1}{2}P\left(\frac{1}{2},\frac{z^2}{2}\right) & \text{if } z<0\end{cases} \quad (10)$$

where:

F(*z*) - cumulative distribution function of the standard normal distribution, *P* (*a, x*) - regularized incomplete gamma function, *z* - standardized value (*z* = (*x*-*μ*) / *σ*) indicates how far a value *x* is from the mean *μ*, expressed in units of standard deviation *σ*.

The incomplete gamma function is a gamma function bounded by an upper bound of *x*. The term "regularized" means that the function is scaled (normalized) to the interval [0,1], so that its value can be viewed as a probability or a relative fraction of the area under the density function.

3.5. Beta distribution

The probability density function of the beta distribution is represented by the following equation [22]:

$$f(x;\mathrm{p},\mathrm{q})=\frac{1}{B(p,q)}x^{p-1}(1-x)^{q-1} \quad (11)$$

where:

p - parameter of form 1, (*p* > 0), *q* - parameter of form 2, (*q* > 0), *x* - variable satisfying the condition 0 ≤ *x* ≤ 1, *B* (*p*, *q*) – denotes the beta function defined over the gamma distribution as *B* (*p*, *q*) = *Γ*(*p*)*Γ*(*q*)/*Γ*(*p*+*q*).

The beta distribution with parameters *p* = *q* = 1 reduces to a uniform distribution between zero and one. The cumulative beta distribution function is represented by the following equation [22]:

$$F(x)=\frac{1}{B(p,q)}\int_0^x t^{p-1}(1-t)^{q-1}dt=\frac{B_x(p,\mathrm{q})}{B(p,q)}=I_x(p,q) \quad (12)$$

where:

B_x, I_x - incomplete beta functions.

4. STATISTICAL DATA ANALYSIS

The wind speed data used in this paper were collected at the Rudine wind farm in Croatia. The wind farm is located at Rudine, at an altitude ranging from 280 to 400 m. Wind speed measurements were made using an anemometer placed at a height of 85 m above the ground, with a time resolution of 10 minutes. A total of 630,113 measurements were collected over a one-year period.

For the purposes of the analysis, a representative set of 63,013 records was formed using equidistant sampling, with every tenth data point selected. This approach allows for a reduction in the volume of data while maintaining the representativeness of the analyzed set.

The analysis was performed on data from the WTG 27 wind turbine, collected via the SCADA system.

Based on the formed data set, statistical processing and modeling of the wind speed distribution were performed using several theoretical distribution functions, including Weibull, Rayleigh, gamma, normal and beta distributions. Each of the above distributions is defined by a corresponding set of parameters whose estimation enables the description of the statistical characteristics of wind speed.

In order to assess the quality of the fit of theoretical distributions to empirical data, statistical error criteria were used, namely RMSE and MAE. These indicators allow a quantitative assessment of the deviation between empirical and theoretical values, with smaller RMSE and MAE values indicating better agreement of the model with the actual data.

In the Weibull distribution, it is necessary to determine the shape parameter (c) and the scale parameter (b) in order to calculate the probability density function and the cumulative function. To calculate the shape parameter, it is necessary to previously determine the value of the standard deviation (σ) and the mean wind speed ($\bar{u}$) based on a representative data set formed by equidistant sampling. To calculate the scale parameter (b), it is necessary to determine the mean wind speed over a one-year period and previously calculate the shape parameter (c).

When calculating the probability density function and the cumulative function of the Rayleigh distribution, the values of the wind speed and the scale parameter (α) are used. The scale parameter (α) is calculated using the mean wind speed ($\bar{u}$) and the constant π.

When calculating the probability density function and the cumulative gamma distribution function, it is necessary to first determine the values of the shape parameter (k) and the scale parameter (Θ). The shape parameter (k) is obtained by dividing the arithmetic mean of all values by the sample standard deviation, and then squaring the resulting value. The scale parameter (Θ) is obtained by dividing the sample variance by the arithmetic mean of the sample, where the variance is the square of the standard deviation.

After determining the mean wind speed and the sample standard deviation, the probability density function and the cumulative normal distribution function can be calculated.

The probability density function and the cumulative beta distribution function can be calculated after determining the values of the shape parameter 1 (parameter p), the shape parameter 2 (parameter q), the lower bound for the beta distribution (minimum of the interval x_{min}) and the upper bound for the beta distribution (maximum of the interval x_{max}).

In order to assess the deviation between the empirical and theoretical distribution values, statistical error measures are used. In this paper, the measures Root Mean Square Error (RMSE) and Mean Absolute Error (MAE) were applied. These measures allow a quantitative assessment of the accuracy of the distribution model in relation to the observed data. RMSE is represented by the following equation [24]:

$$\mathrm{RMSE} = \sqrt{\frac{1}{n}\sum_{i=1}^{n}\left(y_i - \hat{y}_i\right)^2} \tag{13}$$

where:

$\hat{y}_i$ - value of empirical cumulative distribution function, y_i - value of cumulative Weibull distribution function and n - sample size.

MAE is represented by the following equation [24]:

$$\mathrm{MAE} = \frac{1}{n}\sum_{i=1}^{n}\left|y_i - \hat{y}_i\right| \tag{14}$$

Smaller values of RMSE and MAE indicate better agreement between the theoretical model and empirical data. Therefore, the distribution with the smallest values of these criteria is considered the most appropriate for describing the statistical characteristics of wind speed at the observed location.

5. GRAPHIC AND STATISTICAL ANALYSIS OF WIND SPEED DISTRIBUTION

In order to assess the agreement of different statistical distributions with real (empirical) wind speed data, a graphical analysis was first performed. The application of graphical analysis in wind speed modeling in wind energy using different distribution functions is an important step that allows for a direct assessment of the agreement of theoretical distributions with real data and the detection of deviations in certain parts of the wind speed range.

The wind speed histogram, together with the theoretical probability density function curves of different distributions, visually shows the extent to which the theoretical distributions approximate the empirical data. After the visual assessment, a quantitative comparison was performed using RMSE and MAE, which allows for a precise determination of the degree of agreement of each theoretical distribution with the real data. In this way, the combination of graphical and numerical analysis provides a comprehensive insight into the quality of wind speed modeling and identifies the distributions that best describe the empirical distribution.

The wind speed histogram, together with the theoretical probability density function curves of the Weibull, Rayleigh, gamma, normal and beta distributions, is shown in Figure 1.

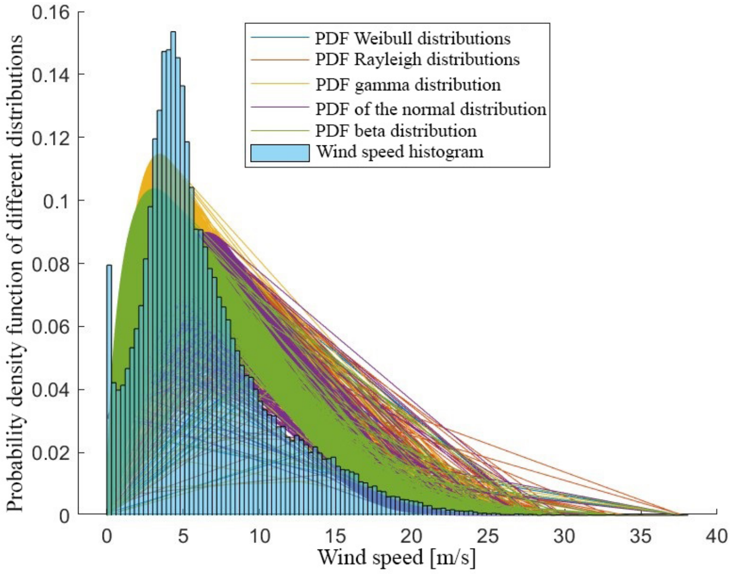

Figure 1: Histogram of wind speeds and curves of theoretical probability density functions of Weibull, Rayleigh, gamma, normal and beta distributions

In Figure 1, the wind speed histogram shows the frequency of occurrence of certain wind speed values in the observed period. The theoretical probability density functions of various statistical distributions, shown in Figure 1 together with the wind speed histogram, represent mathematical models that describe the probability of occurrence of certain wind speeds. The heights of the probability density functions of various statistical distributions show the probability that wind speeds are in a certain interval, with a higher height of the function indicating a more frequent occurrence of the corresponding wind speeds.

The position of the peak of the probability density function of different statistical distributions corresponds to the most frequent values of wind speed. The width of the probability density function of different statistical distributions shows the range of variations of wind speed, while the end points (tails) of the function reflect the frequency of extreme values of wind speed, i.e. very low or very high speeds.

Comparative analysis of the graphical representations in Figure 1 allows us to assess the degree of compliance of individual distributions with real data, in particular with regard to the shape of the curve, its width and the position of the maximum of the probability density function. This comparison allows us to determine the distribution that most accurately approximates the empirical characteristics of wind speeds at the observed location.

The central part of the wind speed histogram, shown in Figure 1, is most accurately approximated by the probability density functions of the beta and normal (Gaussian) distributions, as confirmed by the values RMSE = 0.3963 for the beta distribution and RMSE = 0.3964 for the normal distribution. Based on the MAE value, the Rayleigh distribution (MAE = 0.2317) best approximates the wind speed histogram.

Although the Weibull distribution is often used in wind speed analysis, in this case it did not show the best agreement with the empirical data, which can be attributed to its limited flexibility in describing more complex distribution shapes. On the other hand, the beta and normal distributions better approximate the middle part of the distribution, while the Rayleigh distribution gives better results in terms of average deviation, which is confirmed by the RMSE and MAE values. Distributions such as the Weibull and gamma distributions achieve higher MAE values, which indicates their lower suitability for describing empirical data.

For the purpose of modeling wind speeds in wind energy, it is necessary to show a comparison of the empirical cumulative wind speed distribution function with the theoretical cumulative functions of the Weibull, Rayleigh, gamma, normal and beta distributions.

Figure 2 shows the empirical cumulative wind speed distribution function along with the theoretical cumulative Weibull, Rayleigh, gamma, normal and beta distribution functions.

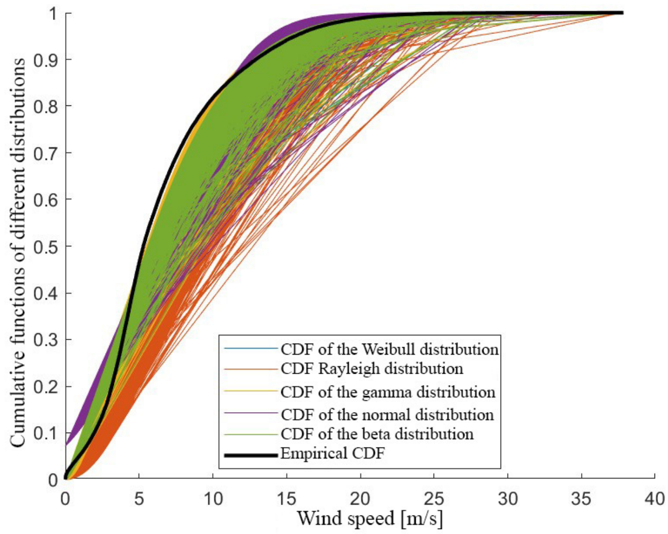

Figure 2: Empirical cumulative wind speed distribution function and theoretical cumulative functions of Weibull, Rayleigh, gamma, normal and beta distributions

The empirical cumulative distribution function of wind speed (empirical CDF) shows the distribution of actually recorded wind speeds. Theoretical cumulative distribution functions show the expected distribution of wind speed values according to the selected statistical distribution (Weibull, Rayleigh, gamma, normal and beta).

The selected theoretical cumulative distribution function shows very good agreement with the empirical cumulative distribution function of wind speed when the deviation between the empirical cumulative distribution function of wind speed and the corresponding theoretical cumulative distribution function is minimal. If the empirical cumulative distribution function of wind speed deviates significantly from the theoretical cumulative functions of all considered distributions, it can be concluded that the selected theoretical cumulative distribution functions do not correspond to the actual data and inadequately approximate the wind speed distribution. In this case, it is necessary to select and apply another theoretical cumulative distribution function in order to achieve a more precise approximation of the actual data.

RMSE and MAE values for different types of distributions are shown in Table 1.

Table 1: Values of RMSE and MAE for different types of distributions

Distribution	RMSE	MAE
Weibull	0.399373271	0.469061626
Rayleigh	0.432387968	0.231695971
Gamma	0.403777638	0.480526376
Normal (Gaussian)	0.396430335	0.395770709
Beta	0.396315358	0.475081171

Analysis of RMSE values shows that the beta distribution and the normal distribution best approximate the empirical cumulative wind speed distribution function shown in Figure 2, almost equally accurately, with the differences in agreement between the theoretical and empirical values being minimal. The MAE values show that the Rayleigh distribution best approximates the empirical cumulative wind speed distribution function shown in Figure 2.

6. CONCLUSION

In this paper, a comparative analysis of five statistical distributions (Weibull, Rayleigh, gamma, normal and beta) was performed in order to model the wind speed distribution based on empirical SCADA data. The analysis included a graphical comparison of probability density functions and cumulative distribution functions, as well as a quantitative evaluation using the statistical criteria RMSE and MAE.

The research results show that the beta and normal distributions achieve the lowest RMSE values, which indicates the best agreement with the empirical cumulative distribution function. On the other hand, the Rayleigh distribution shows the smallest MAE value, indicating the smallest average absolute deviation from the actual data. These results confirm that the choice of the optimal distribution depends on the evaluation criteria, and that different distributions may be more suitable for different aspects of modeling.

Based on the conducted analysis, it can be concluded that the application of statistical distribution functions represents an effective approach in modeling wind speed and assessing wind energy potential. The application of appropriate distributions contributes to the reduction of technical and economic uncertainties, optimization of system operation and achieving higher energy efficiency.

The limitation of this work is reflected in the analysis of data from one location and one time period, which may affect the general applicability of the obtained results. Future research may include the analysis of longer time series of data, as well as the comparison of a larger number of locations in order to obtain more comprehensive conclusions.

REFERENCES

[1] W. Ji, R. Li, W. Xue, Z. Cao, H. Yang, Q. Ning, X. Hu, and G. Liao, "Evaluation of ERA5 wind parameter with in-situ data offshore China", PLoS ONE, Vol. 20 (5), p. e0317751, https://doi.org/10.1371/journal.pone.0317751, (2025)

[2] M. Ćalasan, S. Vujošević, and G. Krunić, "Towards enhanced photovoltaic modeling: New single diode model variants with nonlinear ideality factor dependence", Engineering Science and Technology, an International Journal, Vol. 65, p. 102037, https://doi.org/10.1016/j.jestch.2025.102037, (2025)

[3] E. Chiodo, B. Diban, G. Mazzanti, and F. De Angelis, "A review on wind speed extreme values modeling and Bayes estimation for wind power plant design and construction", Energies, Vol. 16 (14), p. 5456, https://doi.org/10.3390/en16145456, (2023)

[4] D. Erdoğan, K. Yiğit, and B. Acarkan, "Bir rüzgâr enerji santralinin güç kapasitesine bağlı olarak üretebileceği elektrik enerjisi potansiyelinin belirlenmesi – Artvin ili örneği [Determination of the electrical energy production potential of a wind power plant depending on the power capacity: A case study for province of Artvin]", Journal of the Institute of Science and Technology, Vol. 11 (2), pp. 998–1013, https://doi.org/10.21597/jist.852919, (2021)

[5] Z. R. Shu and M. Jesson, "Estimation of Weibull parameters for wind energy analysis across the UK", Journal of Renewable and Sustainable Energy, Vol. 13 (2), p. 023303, https://doi.org/10.1063/5.0038001, (2021)

[6] E. Dokur, S. Ceyhan, and M. Kurban, "Analysis of wind speed data using Finsler, Weibull, and Rayleigh distribution functions", Electrica, Vol. 22 (1), pp. 52–60, https://doi.org/10.5152/electrica.2021.21044, (2022)

[7] P. V. Sireesha and T. Sandhya, "Statistical analysis of wind power density using different mixture probability distribution functions in coastal region of Andhra Pradesh", Electrical Engineering, Vol. 106 (3), pp. 3061–3082, https://doi.org/10.1007/s00202-023-02104-x, (2024)

[8] G. Krunić and S. Vasković, "Wind power plants", Faculty of Production and Management Trebinje, Trebinje (Bosnia and Herzegovina), (2022)

[9] Z. Toor, H. M. Bahaidarah, M. E. Zayed, S. Rehman, V. Khanna, and S. M. Shalaby, "Experimental investigation and CFD modeling on rooftop vertical axis wind turbine for sustainable residential buildings: Development of core design optimization and advanced performance analysis", Energy and Buildings, Vol. 353, p. 116901, https://doi.org/10.1016/j.enbuild.2025.116901, (2025)

[10] Z. Wang and W. Liu, "Wind energy potential assessment based on wind speed, its direction and power data", Scientific Reports, Vol. 11, p. 16879, https://doi.org/10.1038/s41598-021-96376-7, (2021)

[11] S. I. Abood and J. Fuller, "Power system protection and relaying: Computer-aided design using SCADA technology", CRC Press, Boca Raton, FL (USA), https://doi.org/10.1201/9781003394389, (2024)

[12] I. Delgado and M. Fahim, "Wind turbine data analysis and LSTM-based prediction in SCADA system", Energies, Vol. 14 (1), p. 125, https://doi.org/10.3390/en14010125, (2021)

[13] L. Fortuna, G. Nunnari, and S. Nunnari, "Nonlinear modeling of solar radiation and wind speed time series", Springer, Cham (Switzerland), https://doi.org/10.1007/978-3-319-38764-2, (2016)

[14] IPZ Uniprojekt TERRA d.o.o., "Elaborat zaštite okoliša: Izmjena tehničkog rješenja za vjetroelektrane Rudine, općina Dubrovačko primorje, Dubrovačko-neretvanska županija – ocjena o potrebi procjene utjecaja na okoliš", Vjetroelektrana Rudine d.o.o., Zagreb (Croatia), (2020)

[15] J. A. Burgos-Peñaloza, A. A. Lambert-Arista, O. R. García-Cueto, N. Santillán-Soto, E. Valenzuela, and D. E. Flores-Jiménez, "Comparative analysis of estimated small wind energy using different probability distributions in a desert city in northwestern México", Energies, Vol. 17 (13), p. 3323, https://doi.org/10.3390/en17133323, (2024)

[16] P. A. Amaya-Martínez, A. J. Saavedra-Montes, and E. I. Arango-Zuluaga, "A statistical analysis of wind speed distribution models in the Aburrá Valley, Colombia", CT&F – Ciencia, Tecnología y Futuro, Vol. 5 (5), pp. 121–136, https://doi.org/10.29047/01225383.36, (2014)

[17] I. Gordon, "Continuous probability distributions – A guide for teachers (Years 11–12)", Education Services Australia, Melbourne (Australia), (2013)

[18] T. Akman, H. H. Sayan, and Y. Söyletmez, "Estimation of wind power probability density distribution functions parameters by using meta-heuristic algorithms", Gazi Journal of Engineering Sciences, Vol. 10 (2), pp. 329–346, https://doi.org/10.30855/gmbd.0705A12, (2024)

[19] O. Mykhailenko, N. Karabut, V. Doskoch, O. Burtseva, V. Kuznetsov, S. Tsvirkun, and H. Kolomits, "Modeling of wind speed distribution in urban environment for the application of wind energy potential estimation: Case study", TEM Journal, Vol. 14 (1), pp. 107–116, https://doi.org/10.18421/TEM141-10, (2025)

[20] M. Rahman and L. M. Pearson, "A note on estimating parameters in the two-parameter Weibull distribution", Journal of the Korean Data & Information Science Society, Vol. 14 (4), pp. 1091–1102, (2003)

[21] C. D. Lai, D. N. P. Murthy, and M. Xie, "Weibull distributions and their applications", in: H. Pham (Ed.), Springer Handbook of Engineering Statistics, Springer, London (England), pp. 63–78, https://doi.org/10.1007/978-1-84628-288-1_3, (2006)

[22] C. Walck, "Hand-book on statistical distributions for experimentalists", Internal Report SUF-PFY/96-01, University of Stockholm, Stockholm (Sweden), https://staff.fysik.su.se/~walck/suf9601.pdf, (2007)

[23] P. E. Johnson, "Gamma distribution", University of Kansas, Lawrence, KS (USA), https://pj.freefaculty.org/guides/stat/Distributions/DistributionWriteups/Gamma/Gamma-02.pdf, (2013)

[24] T. O. Hodson, "Root-mean-square error (RMSE) or mean absolute error (MAE): When to use them or not", Geoscientific Model Development, Vol. 15 (14), pp. 5481–5487, https://doi.org/10.5194/gmd-15-5481-2022, (2022)

ORIGINAL SCIENTIFIC PAPER OPEN ACCESS

Design and calculation of test stand for testing personal fall protection equipment according to EN 364

Milan Bižić[1*], Dragan Petrović[1]

[1] University of Kragujevac, Faculty of Mechanical and Civil Engineering in Kraljevo, Serbia

ARTICLE INFO

* **Correspondence:** bizic.m@mfkv.kg.ac.rs

DOI: https://doi.org/10.5937/engtoday2600013B

UDC: 621(497.11) **ISSN:** 2812-9474

Article history: Received 9 April 2026; Revised 22 May 2026; Accepted 28 May 2026

ABSTRACT

This paper presents the design and calculation of a test stand intended for testing personal fall protection equipment in accordance with the requirements of the international standard EN 364. The objective of the study was to develop a reliable, safe, and structurally adequate test stand capable of performing both static and dynamic tests on components of fall arrest systems, including different types of personal fall protection systems, fall-arresters, anchor lines, safety harnesses, lanyards, energy absorbers, and connecting elements. The paper analyzes the requirements of EN 364 and defines the functional and structural characteristics of the test stand. Particular emphasis was placed on the static strength of the supporting structure, which was designed to withstand the maximum prescribed test forces without permanent deformation or structural failure, ensuring an adequate safety factor under the most unfavorable loading conditions. Furthermore, the dynamic performance of the test stand was analyzed through the evaluation of its natural frequencies, in accordance with standard requirements. The obtained calculation results confirm that the designed test stand fully complies with the requirements of EN 364 and enables accurate, reliable, and safe testing of personal fall protection equipment, thereby contributing to improved occupational safety and compliance with relevant standards.

KEYWORDS

Personal fall protection equipment, Test stand design, EN 364 standard, Fall arrest system.

1. INTRODUCTION

Fall protection and the prevention of injuries resulting from falls from height are key elements of occupational safety, particularly in industries such as construction, maintenance, and industrial operations where working at height is frequent. Personal protective equipment designed for fall protection, such as full-body harnesses, lanyards, energy absorbers, anchor devices, fall-arresters, is intended to reduce the risk of serious injury during fall events and to ensure compliance with safety regulations and standards [1-3].

Standardized methods of experimental testing are essential for verifying the performance of fall protection equipment and ensure its reliability under both static and dynamic loads. The European standard EN 364 (Personal protective equipment against falls from a height - Test methods) defines procedures for static loading, dynamic impact tests, and other conditioning tests used to evaluate the structural and dynamic characteristics of personal protective equipment components and assemblies used in fall arrest systems [4]. The standard also provides a technical foundation for testing laboratories, manufacturers, and certification bodies to assess personal protective equipment performance, safety, and conformity. It specifies standardized test procedures including static strength assessments, dynamic impact tests using torso dummies, corrosion and environmental conditioning tests, and endurance tests. The standard also provides recommendations for specimen preparation and test scheduling to ensure repeatability and comparability of results.

Scientific research and publications in this field are relatively limited and primarily focus on numerical and experimental investigations of forces, energy absorption, and deformation in personal fall arrest systems under static and dynamic loading conditions. Pomares et al. [5] conducted dynamic tests on fall arrest lanyards and showed that high loading rates significantly reduce resistance compared with static tests, highlighting the need for dynamic test requirements in standards such as EN 354 and EN 364. Carrión et al. [6] conducted dynamic tests on models of Energy Absorber Lanyards from six manufacturers to study their real elongation behavior during fall arrest. Using image processing, they measured the total elongation (elastic and plastic) of each lanyard and determined the minimum clearance distance required to safely arrest a fall without hitting the ground. Pomares et al. [7] conducted both static and dynamic tests on various personal fall arrest devices to evaluate their performance under different fall factors and fall heights. The tests were carried out in accordance with EN 354, EN 355, EN 362, EN 363, and 364 standards, with the aim of analyzing the variables affecting system behavior and energy absorption during fall arrest. Pan et al. [8] developed a multibody dynamic model of a scissor lift and a human operator, and conducted manikin drop tests to evaluate lift stability and the performance of various fall-arrest harnesses and lanyards under simulated fall arrest conditions. The study quantified dynamic loading on the operator model, particularly to the head and neck, while constraining tests to flat surfaces to isolate the effect of manikin-lanyard interaction. Bižić and Petrović [9] provided a systematic overview of the methodology for testing guided-type fall-arresters with a rigid rail anchor line, following the EN 353-1 standard. Their study analyzed the physical, geometric, and mechanical characteristics of the equipment and detailed procedures for performing both static and dynamic tests, based on experiments conducted.

Thus, scientific studies, technical publications, and other literature provide comprehensive guidance on fall protection principles, hazard identification, personal protective equipment selection, and safety management practices [10]. While they emphasize standardized testing and the importance of test stands for evaluating fall protection equipment, practically no publications provide detailed designs or concrete solutions for test stands. Consequently, standards and academic research mainly define general requirements, leaving the practical design and implementation of robust test stands largely to manufacturers and testing laboratories.

In line with the above, this paper presents the design and structural calculation of a dedicated test stand for personal fall protection equipment, fully compliant with European standard EN 364. The test stand enables reproducible static and dynamic testing of various fall protection components, including harnesses, lanyards, energy absorbers, anchor lines, fall-arresters, and connectors. The study integrates both static strength verification and dynamic performance assessment, including evaluation of natural frequencies to prevent resonance during testing. The given test stand represents a practical, safe, and standards-compliant solution for laboratories, manufacturers, and certification bodies, thereby contributing to improved occupational safety and regulatory compliance.

2. MAIN REQUIREMENTS OF STANDARD EN 364

The test stand must be designed to ensure reliable, repeatable, and safe testing of personal fall protection equipment under both static and dynamic conditions. It shall comply with standard EN 10002-2 [11], while force measuring devices used during testing must be calibrated by an authorized accredited laboratory to ensure the required measurement accuracy [4]. The loading rate depends on the material type – for metallic materials, the rate prescribed in standard EN 10002-1 [12] shall be applied, whereas for textile components with a length of 1÷2 meters, the crosshead speed during tests should be 50÷150 mm/min. Controlling the loading rate is very important, as it affects the measured mechanical response of the material and ensures comparability between different tests.

Special attention should be given to the standard's requirements regarding the static and dynamic strength of the test stand's supporting structure. Namely, the structure must be designed so that the application of a 20 kN force at the anchorage point at the top of the test stand does not produce a vertical deflection greater than 1.0 mm. In addition, the natural frequency in the vertical direction at the anchorage point must not be less than 100 Hz [4]. These requirements minimize test stand deformation and dynamic interference, ensuring that test results accurately reflect the behavior of the tested personal protective equipment, rather than the test stand.The anchorage point shall be either a ring with a bore of 20±1 mm or a cross-sectional diameter of 15±1 mm, or a rod of the same cross-sectional diameter. The height of the rigid anchorage point must ensure that no part of the tested system or component, nor the torso dummy or rigid steel mass, comes into contact with the floor during testing.

3. DESIGN AND CALCULATION OF TEST STAND

For the purpose of testing personal fall protection equipment, a special test stand was designed in accordance with the requirements of the EN 364 standard. The supporting structure of the test stand was designed as a closed spatial frame – truss structure made of welded steel box sections. The designed height of the supporting structure, i.e. test stand, is 6.8 m, while the designed base dimensions are 3.0×2.2 m. The structural material specified for the test stand construction is structural steel S235JR. The total mass of supporting structure is about 1.3 t.

At the top of the supporting structure, a special crossbeam is designed, with an anchorage point located on its underside. The crossbeam is movable along its supports, and the element carrying the anchorage point is also movable along the crossbeam itself. In this way, the anchorage point can be positioned at any location within the base area of the test stand, which is of great importance for testing different types of personal fall protection equipment. It should be noted that the test stand is designed to be anchored to the floor at four points, as well as anchored to a fixed wall at the rear side. The appearance of the designed supporting structure of the test stand is shown in Fig. 1.

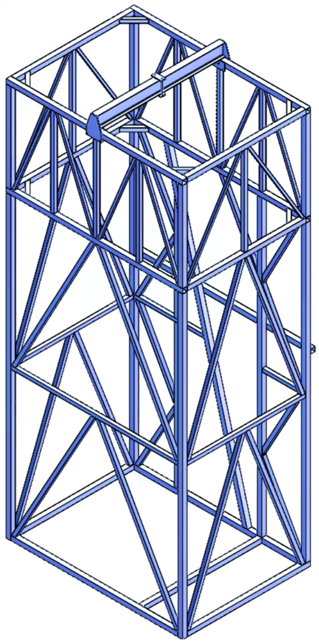

Figure 1: Designed supporting structure of test stand

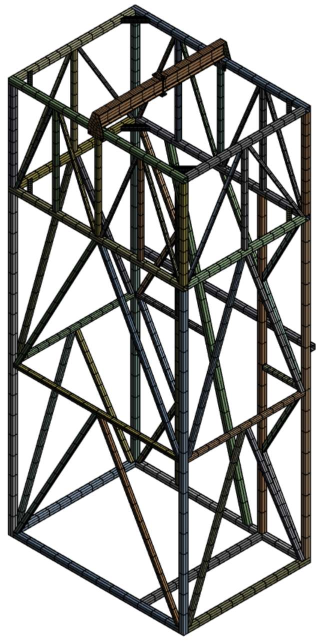

Figure 2: FEM model (65873 nodes, 10682 finite elements)

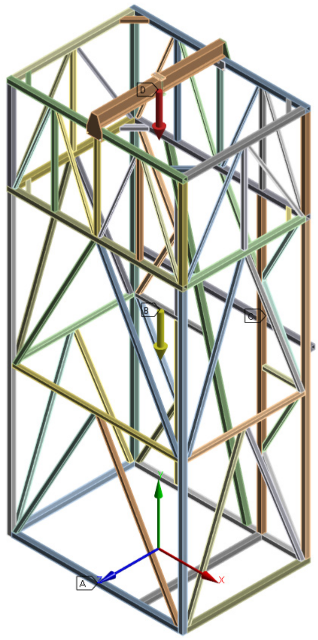

Figure 3: Loads and boundary conditions in model

In order to verify compliance with the requirements of the EN 364 standard, a structural analysis of the supporting structure of the test stand was performed using the finite element method (FEM). By spatial discretization of the supporting structure, a discretized model was created consisting of 65873 nodes and 10682 finite elements (Fig. 2). Boundary conditions in the FEM model were defined in accordance with the actual anchoring method of the test stand: the floor contact surface was modeled as fixed, the two rear wall anchor points prevented displacements normal and transverse to the wall while allowing vertical displacement, and all welded joints were treated as rigid connections.

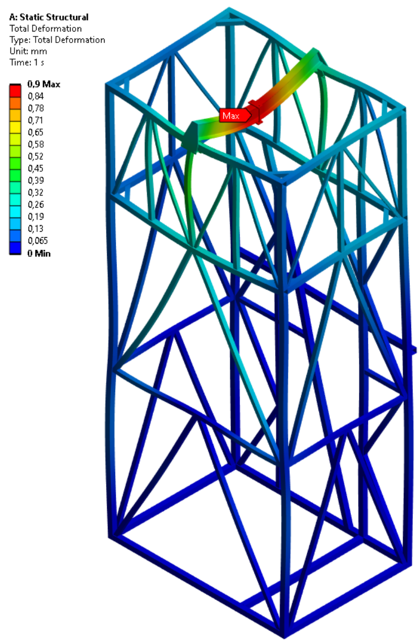

Figure 4: Total deformations of test stand supporting structure

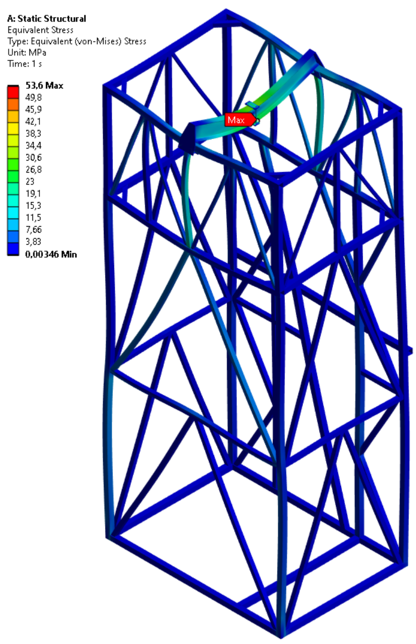

Figure 5: Equivalent stress of test stand supporting structure

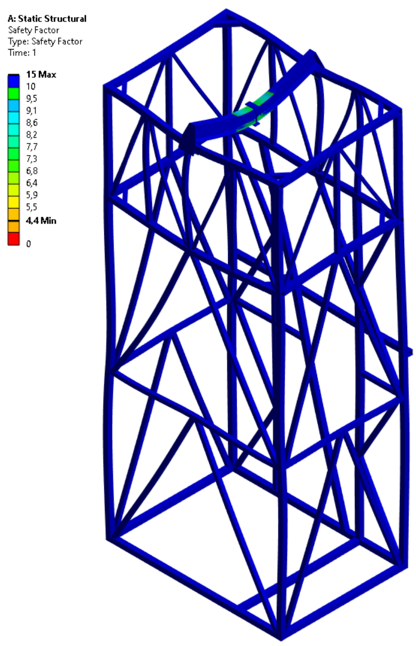

Figure 6: Safety factor of test stand supporting structure

The stress-strain analysis was performed for the critical loading case, where a force of 20 kN acts at the midpoint of the span of the load-bearing crossbeam, while the crossbeam is positioned at the center of the device (Fig. 3). The obtained FEM results for total deformations, stress distribution, and safety factor of the supporting structure of the test stand are presented in Figs. 4–6. For the specified critical loading case, the total deformation at the anchorage point is 0.9 mm in vertical direction, while the equivalent stresses in the supporting structure of the test stand are significantly lower than the allowable stresses; consequently, the safety factor is significantly greater than 1.

Subsequently, a modal analysis was performed to determine the natural frequencies of the first 30 vibration modes of the supporting structure of the test stand. The results of the analysis showed that there are no natural frequencies below 100 Hz for which the anchorage point exhibits dominant oscillations in the vertical direction. The part of the results of the modal analysis are presented in the following figs 7–21.

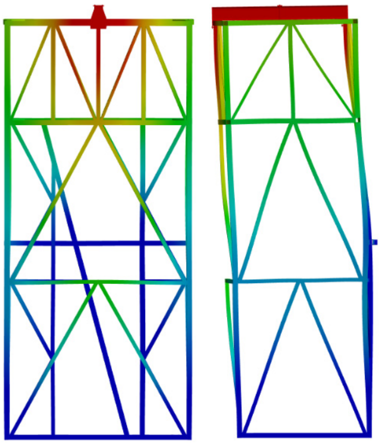

Figure 7: Vibration mode 1 (f_1=18.12 Hz)

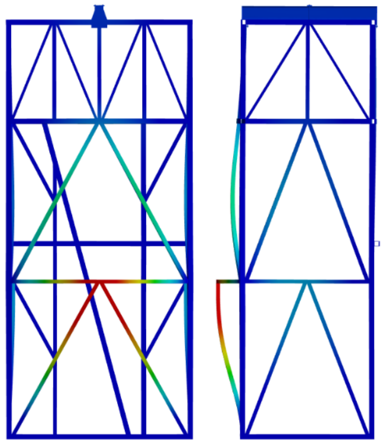

Figure 8: Vibration mode 2 (f_2=24.11 Hz)

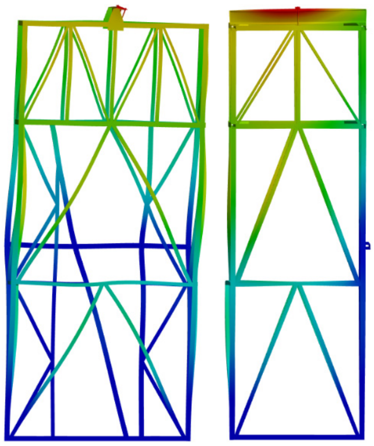

Figure 9: Vibration mode 3 (f_3=24.87 Hz)

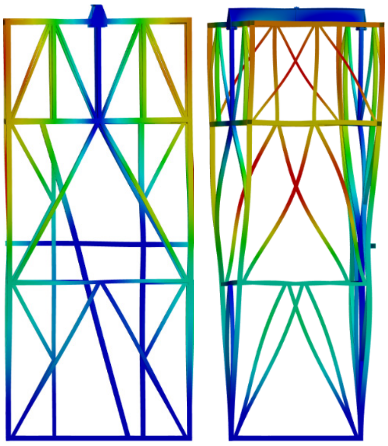

Figure 10: Vibration mode 4 (f_4=29.79 Hz)

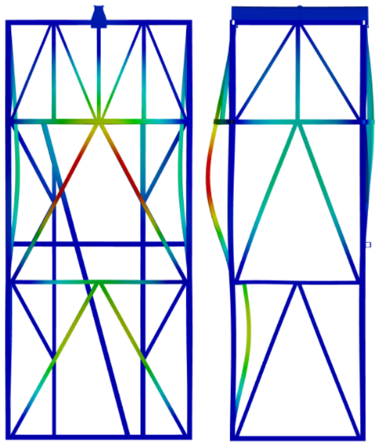

Figure 11: Vibration mode 5 (f_5=30.59 Hz)

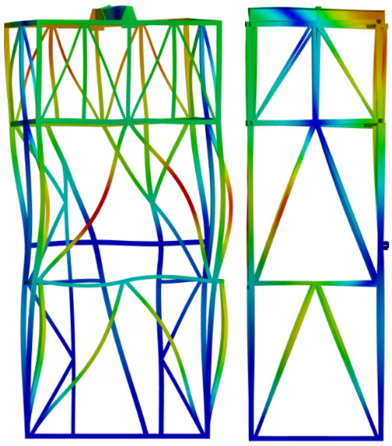

Figure 12: Vibration mode 6 (f_6=34.87 Hz)

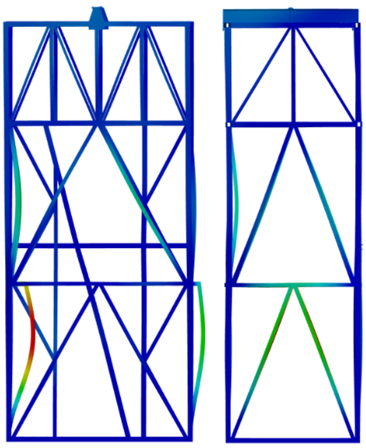

Figure 13: Vibration mode 7 (f_7=35.97 Hz)

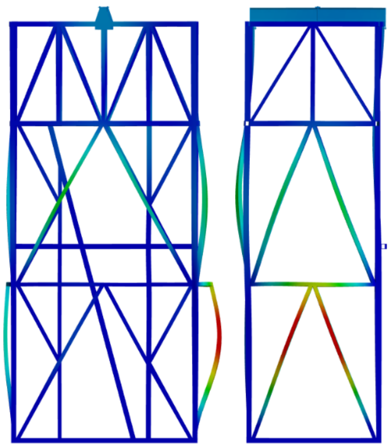

Figure 14: Vibration mode 8 (f_8=36.55 Hz)

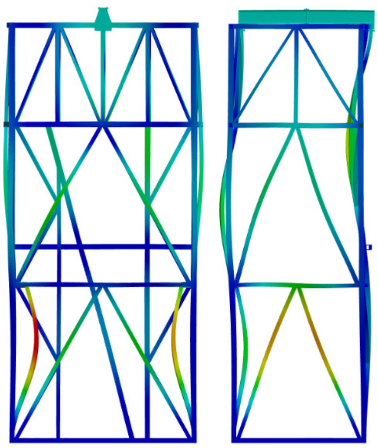

Figure 15: Vibration mode 9 (f_9=37.30 Hz)

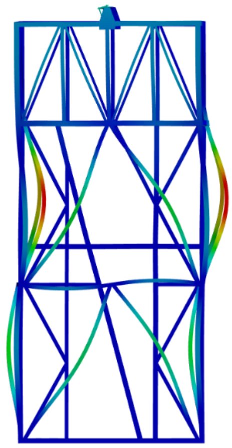

Figure 16: Vibration mode 10 (f_{10}=41.54 Hz)

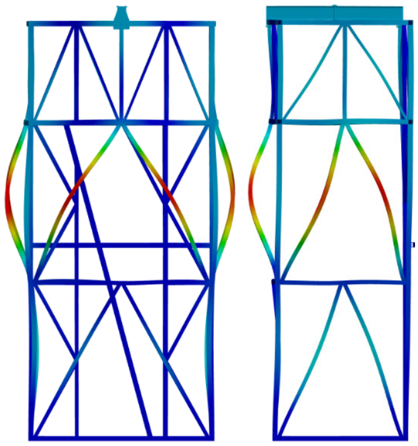

Figure 17: Vibration mode 11 (f_{11}=42.48 Hz)

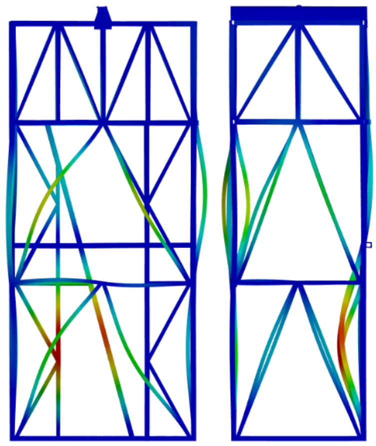

Figure 18: Vibration mode 12 (f_{12}=44 Hz)

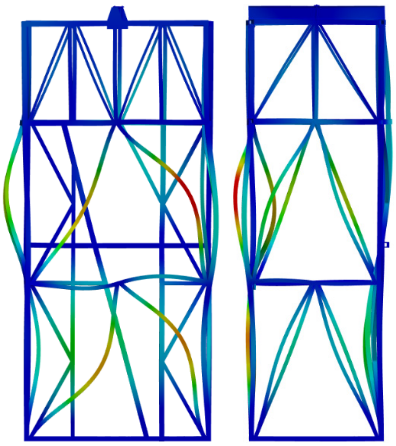

Figure 19: Vibration mode 13 (f_{13}=44.28 Hz)

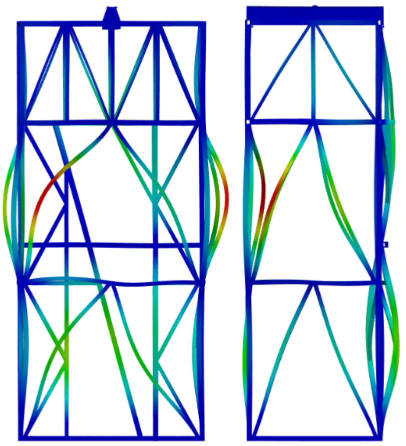

Figure 20: Vibration mode 14 (f_{14}=45.5 Hz)

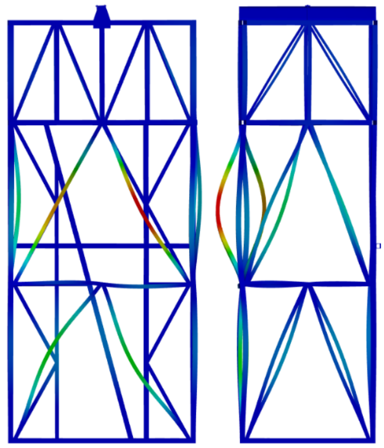

Figure 21: Vibration mode 15 (f_{15}=45.97 Hz)

4. REALIZED TEST STAND

The designed test stand was manufactured in accordance with the developed technical documentation. During fabrication, particular attention was paid to achieving a high structural quality of the test stand, including geometric accuracy, connection details, anchoring to the ground and wall, quality of welded joints, corrosion protection, etc.

Figure 22: Manufactured test stand in operational condition

The test stand is configured to enable safe and controlled execution of standardized tests of personal fall protection equipment. It is equipped with a lifting device for handling test masses and tested equipment, as well as all other necessary auxiliary equipment required for proper test preparation and execution. The geometry and layout of the structure ensure sufficient clearance for test masses and torso dummies, while the adjustable anchorage point allows adaptation to different test configurations. The manufactured test stand in its operational condition is shown in Fig. 22.

5. CONCLUSION

The design, structural analysis, and realization of the test stand for personal fall protection equipment have been successfully completed. The stand provides a safe, stable, and flexible platform for conducting both static and dynamic tests in full compliance with EN 364. Particular attention during fabrication ensured high structural quality, including geometric accuracy, connection details, anchoring, weld integrity, and corrosion protection. The inclusion of a lifting device and all necessary auxiliary equipment enables safe handling of test masses and tested components.

The realized test stand allows reproducible and controlled testing of various fall protection systems, including harnesses, lanyards, energy absorbers, anchor lines, fall-arresters, and anchor devices. By providing reliable and consistent testing conditions, it facilitates the verification of personal protective equipment performance and contributes to enhanced occupational safety.

ACKNOWLEDGEMENTS

The authors are grateful to the Ministry of Science, Technological Development and Innovation of the Republic of Serbia for support (contract no. 451-03-34/2026-03/200108).

REFERENCES

[1] N. Krishnamurthy, "Safety at height: A holistic view of fall management", CRC Press, Taylor & Francis Group, Boca Raton, FL (USA), https://doi.org/10.1201/9781032648132, (2024)

[2] H. Hsiao, "Fall prevention and protection: Principles, guidelines, and practices", CRC Press, Taylor & Francis Group, Boca Raton, FL (USA), https://doi.org/10.1201/9781315373744, (2017)

[3] G. Drennan Gagnet and M. Drennan, "Fall protection and scaffolding safety: An illustrated guide", Government Institutes, Rockville, MD (USA), (2000)

[4] BS EN 364:1993, "Personal protective equipment against falls from a height - Test methods", British Standards Institution, (1993)

[5] J. C. Pomares, E. Á. Carrión, A. González, and P. I. Saez, "Optimization on personal fall arrest systems. Experimental dynamic studies on lanyard prototypes", International Journal of Environmental Research and Public Health, Vol. 17(3), p. 1107, https://doi.org/10.3390/ijerph17031107, (2020)

[6] E. Á. Carrión, B. Ferrer, J. F. Monge, P. I. Saez, J. C. Pomares, and A. González, "Minimum clearance distance in fall arrest systems with energy absorber lanyards", International Journal of Environmental Research and Public Health, Vol. 18(11), p. 5823, https://doi.org/10.3390/ijerph18115823, (2021)

[7] J. C. Pomares, E. Á. Carrión, R. Irles, A. González, and E. G. Segovia, "Experimental tests on personal safety devices for falls from height", WIT Transactions on the Built Environment, Vol. 180, pp. 69–81, https://doi.org/10.2495/SUSI180071, (2018)

[8] C. S. Pan, J. R. Powers, J. J. Hartsell, J. R. Harris, B. M. Wimer, R. G. Dong, and J. Z. Wu, "Assessment of fall-arrest systems for scissor lift operators: Computer modeling and manikin drop testing", Human Factors, Vol. 54(3), pp. 358–372, https://doi.org/10.1177/0018720811425024, (2012)

[9] M. Bižić and D. Petrović, "Methodology of testing guided-type fall arresters with rail-based rigid anchor lines", Engineering Today, Vol. 4(1), pp. 31–40, https://doi.org/10.5937/engtoday2500005B, (2025)

[10] J. N. Ellis, "Introduction to fall protection", American Society of Safety Engineers, IL (USA), (2001)

[11] BS EN 10002-2:1992, "Metallic materials - Tensile testing - Part 2: Verification of the force measuring system of the tensile testing machines", British Standards Institution, https://doi.org/10.3403/00263687, (1992)

[12] BS EN 10002-1:1990, "Metallic materials- Tensile testing - Part 1: Method of test at ambient temperature", British Standards Institution, (1990)

ORIGINAL SCIENTIFIC PAPER OPEN ACCESS

Risks and safety management in photovoltaic systems

Goran Bošković*[1], Željana Kužet[2], Bojana Zoraja[2], Vladimir Mučenski[2], Zoran Čepić[2]

[1] University of Kragujevac, Faculty of Mechanical and Civil Engineering, Kraljevo, Serbia

[2] University of Novi Sad, Faculty of Technical Sciences, Novi Sad, Serbia

ARTICLE INFO

* **Correspondence:** boskovic.g@mfkv.kg.ac.rs

DOI: https://doi.org/10.5937/engtoday2600014B

UDC: 621(497.11) **ISSN:** 2812-9474

Article history: Received 27 April 2026; Revised 2 June 2026; Accepted 10 June 2026

ABSTRACT

The application of solar photovoltaic systems has experienced significant growth in recent years, resulting in an increasing number of workers involved in the design, installation, operation, and maintenance of solar power plants. Although solar technology is generally considered relatively safe during operation, certain stages of its life cycle involve specific occupational health and safety (OHS) risks. This paper aims to present and systematize the key risks and protective measures in the field of solar energy through a review of scientific literature, technical reports, and relevant standards. The research methodology is based on the qualitative analysis and classification of hazards identified during different phases of solar power plant operation. The results indicate that the most common risks are associated with working at heights, exposure to direct current electrical hazards, and the influence of climatic and organizational factors. Particular emphasis is placed on the implementation of safe work procedures, the use of appropriate personal protective equipment, continuous worker training, and the introduction of safety management systems in accordance with international standards. It is concluded that effective OHS risk management requires an integrated approach combining technical, organizational, and educational measures aimed at reducing workplace injuries and improving safety in the solar industry.

KEYWORDS

Solar photovoltaic systems, Risks, Protective measures, Renewable energy sources, Occupational safety management

1. INTRODUCTION

Photovoltaic systems today represent one of the fastest-growing sources of renewable energy worldwide and play a significant role in the global energy transition. Continuous technological progress, declining costs of solar module production, and the increasing need to reduce greenhouse gas emissions have contributed to the intensive development and widespread application of solar technologies in industry, public infrastructure, and households. Owing to their ability to generate electricity without the direct combustion of fossil fuels, photovoltaic systems are widely regarded as one of the key solutions for achieving sustainable energy development and mitigating the environmental impact of the energy sector [4–6].

However, despite the numerous advantages of solar energy, recent studies indicate that the application of photovoltaic systems is not entirely risk-free. Risks associated with these systems cover a broad range of technical, health, environmental, and social aspects that arise throughout the entire life cycle of the equipment—from manufacturing and transportation, through installation and operation, to maintenance, recycling, and final disposal of panels [4–6]. Particular attention is given to electrical hazards, the potential for fire incidents, working at heights during installation and maintenance, as well as possible exposure to hazardous chemical substances present in certain components of solar modules. In addition, the growing number of decommissioned and damaged panels raises concerns regarding adequate waste management and the development of efficient recycling systems, representing a significant challenge for the long-term sustainability of the solar industry [11, 12].

In addition to technical and environmental aspects, increasing importance is also attributed to social factors related to working conditions, production organization, and global supply chains. Contemporary safety approaches emphasize that the sustainability of photovoltaic systems cannot be assessed solely through energy efficiency or emission reduction, but must also consider their impact on worker health, the quality of working conditions, and the broader social environment [7, 10].

Previous research has mostly focused on individual aspects of safety and sustainability, with the majority of studies analyzing technical failures, electrical hazards, or environmental impacts separately. A significantly smaller number of studies have attempted to integrate multiple risk dimensions into a unified analytical framework to understand their interrelationships [8, 13]. Therefore, this paper aims to systematize existing knowledge through a comprehensive literature review and present the development of risk understanding in photovoltaic systems—from earlier studies focused on isolated technical issues to contemporary integrated approaches that link technical, health, environmental, and social aspects of risk management.

2. DEVELOPMENT OF RESEARCH THROUGH THE LITERATURE

2.1. Initial Research on Environmental Risks (2000–2014)

One of the earliest studies highlighting potential negative impacts of photovoltaic systems was the work of Fthenakis and Moskowitz [4] in 2000, which emphasized that the production of solar cells may involve hazardous materials such as cadmium, lead, and various industrial gases. The authors demonstrated that environmental impacts should not be considered only during system operation, but across the entire life cycle of the equipment.

Later, Bakhiyi et al. [5] in 2014 expanded this perspective by analyzing the impact of the photovoltaic industry on worker health. Their study highlighted the significance of chemical exposure during manufacturing processes, as well as the need for stricter industrial safety procedures.

2.2. Focus on Installation Safety (2017–2021)

White and Doherty [1] pointed out that photovoltaic systems present a specific challenge for electrical safety, as the modules remain energized even when the system is formally switched off. They identified the most significant risks as:

- electric shock,
- electrical arc (Fig. 1),
- fire caused by DC installations.

Figure 1: Arc Fault in a Solar Power System

Duroha and Macht [2] in 2023 further analyzed the risks during the installation and maintenance of solar systems. Their results showed that working at heights, manual handling of panels, and heat stress are common causes of occupational injuries in practice. Costa Lima et al. [3] demonstrated that system safety largely depends on the design itself, particularly on the layout of DC wiring and rapid shutdown systems.

2.3. Expansion to Social and Organizational Aspects (2022–2024)

Bonilla-Alicea and Fu [10] in 2022 expanded the research focus from purely technical issues to the social aspects of photovoltaic system implementation. Their analysis indicated that the sustainability of photovoltaic systems also includes issues such as:

- working conditions,
- resource availability,
- regional inequalities

Adekanmbi et al. [6] in 2024 demonstrated that risks associated with photovoltaic systems exist across all phases of the life cycle, from manufacturing to recycling. They particularly emphasized the issue of the growing volume of solar panel waste. At the same time, contemporary HSE approaches [9] highlight the need to integrate health protection, environmental protection, ergonomic principles (Fig. 2), and organizational safety into a unified risk management system.

Figure 2: Example of Work Activities During Photovoltaic System Installation

2.4. Contemporary Trends (2025–2026)

Recent research further shifts the focus from individual hazards toward integrated risk management. Shafira and Abadi [8] in 2025 developed an HSEE approach in which technical and human factors are considered jointly. Studies on waste management [11, 12] emphasize that solar panel recycling is becoming one of the key sustainability issues in the solar industry. Contemporary works [13, 15] highlight the importance of:

- digital monitoring of components,
- supply chain transparency,
- predictive maintenance.

Zafar et al. [7] show that social risks are increasingly becoming as important as technical factors. The regulatory framework [14] further confirms the need for systematic management of waste and hazardous materials.

3. METHODOLOGY

A systematic literature review method was applied in this study, combined with a semi-quantitative risk assessment approach. The literature was collected from relevant scientific databases and analyzed to identify key risks associated with photovoltaic systems.

3.1. Risk Assessment Method

For the assessment of identified risks, a semi-quantitative likelihood–severity matrix method was applied (Likelihood Severity Matrix). The overall risk level was determined as the product of these two parameters:

$$R = P \times S \tag{1}$$

where R is the risk level, P is the probability of occurrence, and S is the severity of the consequence.

3.2. Assessment Criteria

The parameter values were determined based on:

- frequency of occurrence in the literature
- severity of consequences
- the system life cycle phase

3.3. **Determination of probability and consequence parameters**

The values of the probability of risk occurrence (*P*) and severity of consequence (*S*) were determined based on a comparative analysis of findings from available literature. When assigning numerical values, the following were taken into account:

- the frequency of occurrence of a particular risk in the analyzed studies,
- the severity of consequences described in the literature,
- the phase of the life cycle in which the risk occurs,
- the number of authors who identify the same risk as significant.

The probability was estimated based on the relative frequency of risk occurrence in published studies, while the severity of the consequence was determined according to its potential impact on:

- human health,
- system safety,
- the environment,
- organizational sustainability.

In this way, a semi-quantitative assessment was obtained, enabling the comparison of different risk categories within a unified model.

4. CONCEPTUAL FRAMEWORK FOR RISK ASSESSMENT

To systematize the identified hazards, a conceptual framework for the integrated risk assessment of photovoltaic systems was developed, as shown in Figure 3. The proposed model is based on the system life cycle as the fundamental analytical unit and links technical, health-environmental, and social dimensions of risk into a unified assessment approach. In this way, it is possible to consider the interrelationship of different factors that determine the overall level of safety and sustainability of photovoltaic installations.

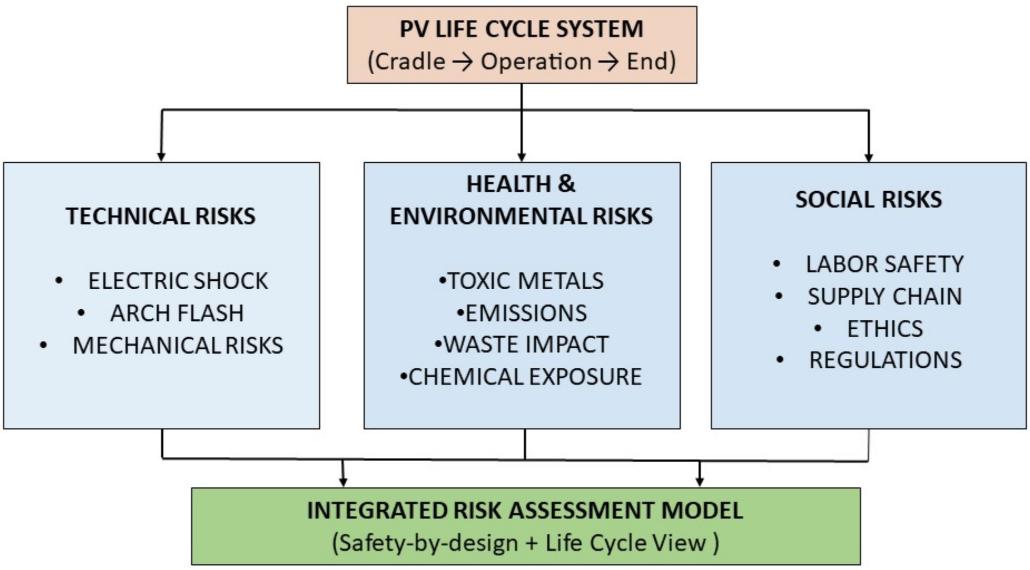

Figure 3: Conceptual framework for integrated risk assessment of photovoltaic systems

The presented model illustrates the interrelationship between technical, health-environmental, and social risks throughout the entire life cycle of a photovoltaic system. The model shows that individual risks do not act in isolation, but rather their interaction determines the overall level of system safety and sustainability.

The proposed conceptual framework shows that risk assessment in photovoltaic systems cannot be based solely on technical parameters. An electrical failure can simultaneously cause worker injury, environmental damage, and economic consequences, while inadequate working conditions can increase the likelihood of technical incidents. For this reason, it is necessary to apply an integrated risk management approach that covers all phases of the system life cycle.

5. RISK ASSESSMENT OF PHOTOVOLTAGE SYSTEMS

Based on the conceptual framework presented in Figure 3, a semi-quantitative assessment of the most significant risks in photovoltaic systems was performed. The assessment was carried out using a risk matrix based on the probability of an adverse event occurring and the severity of its consequences. This approach enables systematic risk ranking and the identification of areas where priority implementation of control measures is necessary.

Table 1: Semi-quantitative risk assessment of photovoltaic systems

Identified risk	Risk category	Probability (P)	Consequence (S)	Risk value (R=P×S)	Risk level	Priority of measures
Electric shock	Technical	3	3	9	Critical	Immediate
Electric arc	Technical	2	3	6	High	High
Fall from height	Operational	3	3	9	Critical	Immediate
Heat stress	Health-related	2	2	4	Medium	Planned
Chemical exposure	Health-environmental	2	3	6	High	High
Waste panels	Environmental	2	3	6	High	High
Inadequate working conditions	Social	2	2	4	Medium	Planned

The values of probability and consequence were determined using a three-level scale, where the value 1 indicates a low level, the value 2 a medium level, and the value 3 a high level of the assessed parameter. The total risk value was obtained as the product of probability and consequence, where a higher value indicates a higher priority for the implementation of preventive measures.

The results presented in Table 1 show that the highest level of risk in photovoltaic systems is represented by electric shock and working at height, which are classified as critical risks due to their high likelihood of occurrence and severe consequences for worker safety [1, 2]. The group of high risks includes electric arc, chemical exposure, and waste panel management, as these can cause long-term negative impacts on human health and the environment [4, 11, 12]. Social factors and heat stress are assessed as medium risks; however, their long-term neglect may indirectly increase the overall level of system safety vulnerability [7, 10].

6. DISCUSSION

The analysis of the available literature shows that risks in photovoltaic systems cannot be adequately assessed if they are considered in isolation, as there is a pronounced interdependence between technical, health, environmental, and organizational factors. Technical failures, such as electric arcs, installation damage, or component overheating, can have direct consequences for worker safety through an increased risk of electric shock, fire, or injuries during system maintenance. At the same time, such incidents can also lead to indirect consequences, including system downtime, economic losses, infrastructure damage, and negative environmental impacts due to the release of hazardous substances or the generation of hazardous waste.

Particularly important is the fact that modern safety management approaches highlight the need for integrating different disciplines in the risk assessment process. Traditional models, which were predominantly focused on the technical reliability of systems, are no longer sufficient for understanding the complexity of modern photovoltaic installations. For this reason, integrated approaches that combine engineering design, occupational health protection, environmental management, and organizational safety procedures are increasingly being applied. Such models enable the timely identification of potential hazards and the development of more effective preventive measures throughout all phases of the system life cycle.

In addition to technical and environmental aspects, social factors are also becoming increasingly important in influencing the overall sustainability of the solar industry. Working conditions during the production, installation, and maintenance of photovoltaic systems directly affect employee safety levels and system reliability during operation. Inadequate worker training, lack of protective equipment, poor work organization, or insufficiently developed regulatory mechanisms can increase the likelihood of incidents and reduce the effectiveness of protective measures. Furthermore, global supply chains and the growing production of solar equipment raise additional issues related to ethical manufacturing, sustainable resource management, and the long-term social responsibility of companies operating in the renewable energy sector.

The obtained results confirm that the sustainability of photovoltaic systems should not be viewed solely through energy efficiency and the reduction of greenhouse gas emissions, but also through the system's ability to simultaneously ensure technical reliability, worker safety, environmental protection, and socially responsible management throughout the entire life cycle.

7. CONCLUSION

Photovoltaic systems represent an important element of the modern energy transition and play a key role in reducing dependence on fossil fuels and achieving sustainable development goals. However, the results of the analyzed literature show that their widespread application simultaneously involves a complex set of interrelated technical, health, environmental, and social risks that arise throughout the entire life cycle of the system. Therefore, the safety and sustainability of photovoltaic systems cannot be viewed solely through energy efficiency or the reduction of greenhouse gas emissions, but require an integrated risk management approach. This paper developed a conceptual model for integrated risk assessment that links different categories of hazards across the stages of production, installation, operation, maintenance, and decommissioning of photovoltaic systems.

A particular contribution of this paper lies in integrating multiple risk assessment approaches into a unified analytical framework that enables a more comprehensive understanding of the interrelationships among technical, organizational, and environmental aspects of photovoltaic systems. Such an approach can serve as a basis for developing more effective safety management strategies, improving regulatory procedures, and implementing more sustainable technologies in the renewable energy sector.

ACKNOWLEDGEMENTS

This work has been supported by the Ministry of Science, Technological Development, and Innovation of the Republic of Serbia, through the Contract for the scientific research financing in 2026, (Contract No. 451-03-34/2026-03/200108 and 451-03-34/2026-03/200156) to build resilient infrastructure, promote inclusive and sustainable industrialization, and foster innovation, which is the ninth goal of the UN's 2030 Agenda of Sustainable Development.

REFERENCES

[1] J.R. White and M. Doherty, "Hazards in the installation and maintenance of solar panels", Proceedings of the 2017 IEEE IAS Electrical Safety Workshop (ESW), pp. 1-5, https://doi.org/10.1109/ESW.2017.7914834, (2017)

[2] J.C. Duroha and G.A. Macht, "Solar installation occupational risks: A systematic review", Safety Science, Vol. 160, p. 106048, https://doi.org/10.1016/j.ssci.2022.106048, (2023)

[3] J.P. Costa Lima, A. da Cunha Lima, L.V. Bellinaso, and L. Michels, "Explanatory review about rapid shutdown systems and standards to increase safety in photovoltaic systems", Proceedings of the 14th Seminar on Power Electronics and Control (SEPOC 2022), pp. 1-5, https://doi.org/10.1109/SEPOC54972.2022.9976424, (2022)

[4] V.M. Fthenakis and P.D. Moskowitz, "Photovoltaics: Environmental, health and safety issues and perspectives", Progress in Photovoltaics: Research and Applications, Vol. 8(1), pp. 27-38, https://doi.org/10.1002/(SICI)1099-159X(200001/02)8:1<27::AID-PIP296>3.0.CO;2-8, (2000)

[5] B. Bakhiyi, F. Labrèche, and J. Zayed, "The photovoltaic industry on the path to a sustainable future—Environmental and occupational health issues", Environment International, Vol. 73, pp. 224-234, https://doi.org/10.1016/j.envint.2014.07.023, (2014)

[6] A.O. Adekanmbi, N. Ninduwezuor-Ehiobu, U. Izuka, A. Abatan, E.C. Ani, and A. Obaigbena, "Assessing the environmental health and safety risks of solar energy production", World Journal of Biology Pharmacy and Health Sciences, Vol. 17(2), pp. 225-231, https://doi.org/10.30574/wjbphs.2024.17.2.0080, (2024)

[7] I. Zafar, V. Stojceska, and S. Tassou, "Social sustainability assessments of industrial level solar energy: A systematic review", Renewable and Sustainable Energy Reviews, Vol. 189, p. 113962, https://doi.org/10.1016/j.rser.2023.113962, (2024)

[8] D.A.I. Shafira and I. Abadi, "A study on health, safety, environment, and ergonomics (HSEE) in solar power plant", Journal of Engineering and Applied Technology, Vol. 6(1), pp. 18-26, https://doi.org/10.21831/jeatech.v6i01.84689, (2025)

[9] S. Mirabal, R. Datar, and A.M. Garcia, "Health, safety and environment (HSE) manual for solar parks in India", Standard Operational Procedures for Solar Parks, Vol. IV, IBF International Consulting, EQO-NIXUS (OCA Global), and IDOM, https://www.eeas.europa.eu/sites/default/files/vol_4_health_safety_and_environment_manual.pdf, (2019)

[10] R.J. Bonilla-Alicea and K. Fu, "Social life-cycle assessment (S-LCA) of residential rooftop solar panels using challenge-derived framework", Energy, Sustainability and Society, Vol. 12, p. 7, https://doi.org/10.1186/s13705-022-00332-w, (2022)

[11] W. Luo, Y.S. Khoo, A. Kumar, J.S.C. Low, Y. Li, Y.S. Tan, Y. Wang, A.G. Aberle, and S. Ramakrishna, "A comparative life-cycle assessment of photovoltaic electricity generation in Singapore by multicrystalline silicon technologies", Solar Energy Materials and Solar Cells, Vol. 174, pp. 157-162, https://doi.org/10.1016/j.solmat.2017.08.040, (2018)

[12] D. Mulvaney, “Solar power: Innovation, sustainability, and environmental justice”, University of California Press, Berkeley (USA), https://doi.org/10.2307/j.ctvd1c6zh, (2019)

[13] Occupational Safety and Health Administration, “Green job hazards-Solar energy”, U.S. Department of Labor, [Online]. Available: https://www.osha.gov/green-jobs/solar

[14] European Parliament and the Council of the European Union, “Directive 2012/19/EU of the European Parliament and of the Council of 4 July 2012 on waste electrical and electronic equipment (WEEE) (recast)”, Official Journal of the European Union, L 197, pp. 38-71, (2012)

[15] A. Louwen and Ch. Schill, “Digitalisation and digital twins in photovoltaic systems”, A. Louwen, Ch. Schill, L.S. Bruckman, and U. Jahn (Eds.), IEA PVPS Task 13, Report No. T13-34:2026, ISBN 978-1-7642902-6-5, https://doi.org/10.69766/RMPH3089, (2026)

Engineering
TODAY

VOL. 5 / NO. 1 / 2026

CONTENTS